Review

The possible role of metal carbonyl clusters in nanoscience and nanotechnologies

Cristina Femoni, M. Carmela Iapalucci, Francesco Kaswalder, Giuliano Longoni *, Stefano Zacchini

Dipartimento di Chimica Fisica ed Inorganica, Università di Bologna, viale Risorgimento 4, 40136 Bologna, Italy

Contents

Abstract

Although a few nanosized metal carbonyl clusters were already obtained in the seventies, these structurally and compositionally well-defined molecules attracted the interest of nanoscientists only as possible precursors of finely dispersed metal particles for heterogeneous catalysis. This review article has the aim to give a brief account of most recent results in the field of high-nuclearity metal carbonyl clusters and their emerging properties. In doing that, a look to related behaviour of ligand-stabilised and ligand-free clusters, including almost mono-dispersed ligand-stabilised metal nanoparticles, is given. At the end, we will deliberately venture in some speculations on the possible contribution of metal carbonyl clusters to some aspects of nanoscience and nanotechnologies.
© 2006 Elsevier B.V. All rights reserved.

Keywords: Metal carbonyls; Clusters; Electrochemical behaviour; Magnetic properties; Functional materials; Nanomaterials

1. Introduction

It has been suggested that metal clusters stabilised in a ligand shell are valid candidates to assemble functional devices for data

* Corresponding author. Tel.: +39 051 20 93711; fax: +39 051 20 93690.
  E-mail address: longoni@ms.fci.unibo.it (G. Longoni).

storage and could potentially represent the ultimate solution for miniaturisation in microelectronics and nanolithography [1–6]. Could metal *carbonyl* clusters (afterwards indicated with the acronym MCC) play a role in this area?

In writing this review, our aim is to try to give a motivated answer to the above question, rather than provide a comprehensive overview of synthetic methods and methodologies, structural and spectroscopic behaviour, bonding theories, chemical and physical properties and catalytic application of MCC. On the above topics there are available excellent books, both at an introductory and specialistic level, dedicated to cluster chemistry and physics in general, and containing chapters or reviews expressly dedicated to MCC [7–16]. Besides, two praiseworthy compilations of all relevant survey bibliography regarding cluster chemistry, MCC included, have already been published [17,18].

The most recent progresses in MCC chemistry and physics allow to envision a potential contribution of MCC to some aspects of nanoscience and nanotechnologies. Therefore, we have chosen to venture in the yet rather speculative territory of MCC as functional molecules in themselves or building blocks to assemble functional materials, as well as their potential use as precursors of the above. We will begin by showing that metal carbonyl clusters are not necessarily close-shell, how they could be tailored to display redox and magnetic behaviour and, eventually, to become multivalent. To this purpose, we will only review the so far reported MCC containing at least one interstitial metal atom. The formal similarity between redox-active MCC and nanocapacitors will be then analysed. Throughout the sections, these emerging properties of molecular MCC will be compared with those of other molecular and non-molecular ligand-stabilised and ligand-free clusters, including almost mono-dispersed ligand-stabilised metal nanoparticles. We will end by surveying 1D and 2D arrays of MCC and making some speculations on the possible contribution of MCC to some aspects of nanoscience and, eventually, nanotechnologies.

2. The development of redox and magnetic behaviour in metal carbonyl clusters

It was a widespread opinion that MCC should adopt close-shell electronic configurations and could exhibit an almost perfect correspondence between number of cluster valence electrons (CVE) and geometry of the metal frame, and vice versa. Countless examples of structurally characterised low-nuclearity MCC lend support to the above belief [7–16]. Rules for electron bookkeeping in MCC have been developed with the support of semiempirical calculations [19–22], which rationalised the relationships between electron count and geometry of most clusters and proved to be extremely useful in designing and making new MCC.

However, as the size of the MCC increases, deviations from the predicted electron count begin to become significant. As it is shown in Fig. 1 just as an example, the range of variation in the number of CVE (ΔCVE) increases from 4 to 12 for tetrahedral clusters of frequency ν_2 and ν_3, whereas all known ν_1-tetrahedral MCC are electron-precise and constantly show 60

Table 1
Some representative examples of MCC displaying two or more reversible redox changes or multivalence

	Compound	n	References
1	$[Fe_5S_2(CO)_{14}]^{n-}$	0, 1, **2**	[43]
2	$[Fe_4Au(CO)_{16}]^{n-}$	**1**, 2, 3	[44]
3	$[Fe_3Pt_3(CO)_{15}]^{n-}$	**0**, **1**, **2**	[45–47]
4	$[Os_4Pt_2(CO)_{17}]^{n-}$	0, 1, 2	[48]
5	$[Ir_6(CO)_{15}]^{n-}$	0, 1, **2**	[49]
6	$[Co_8C(CO)_{18}]^{n-}$	1, **2**, 3, 4	[39]
7	$[H_4Os_{10}(CO)_{24}]^{n-}$	0, 1, **2**	[50]
8	$[Os_{10}C(CO)_{24}]^{n-}$	1, **2**, 3	[50–52]
9	$[HFe_6Pd_6(CO)_{24}]^{n-}$	2, **3**, 4, 5	[53,54]
10	$[Co_{13}C_2(CO)_{24}]^{n-}$	**3**, **4**, 5, 6	[39,55–57]
11	$[Co_{13}N_2(CO)_{24}]^{n-}$	**3**, 4, 5	[57]
12	$[Ir_{14}(CO)_{27}]^{n-}$	0, **1**, 2	[58]

n values in bold indicate the species which have been isolated in a crystalline state and structurally characterised.

CVE. This difference in the number of required CVE is apparently due to the change in atomic properties of the involved metal atoms, which are less relevant in low-nuclearity clusters and become progressively more effective as the size and, consequently, the number of energy levels increase. In agreement with this view, only few stable MCC with an open-shell electronic configuration were known. Indeed, in contrast to high-valent organometallic clusters [32,33], most MCC are close-shell and their redox aptitude is generally rather poor [34–41]. At best only one redox change displays features of chemical reversibility, unless the fortuitous occurrence of miscellaneous "ad hoc" conditions gives rise to sufficiently stable open-shell electronic configurations [42]. Some representative examples of MCC displaying two or more reversible redox changes or multivalence are collected in Table 1. In this context, multivalence has the meaning that a given MCC is stable on the work-up time-scale with different free charges and remains structurally invariant. Inspection of Table 1 indicates that this behaviour can be found in both homo- (three entries) and hetero-metallic (four entries) clusters, as well as in MCC containing main-group interstitial (four entries) or peripheral elements. That is likely to happen due to a synergetic combination of steric and electronic effects, which give rise to a set of "ad hoc" conditions.

As previously pointed out [42], an "ad hoc" condition can consist into a synergy between efficient shielding of the carbonyl shell and presence of one or more orbitals weakly antibonding or non-bonding in a well-defined energy gap (a potential HOMO–LUMO gap), e.g. $[Fe_4Au(CO)_{16}]^-$ [44], $[Fe_3Pt_3(CO)_{15}]^{2-}$ [47], and $[HFe_6Pd_6(CO)_{24}]^{3-}$ [54]. Often these orbitals are amenable to be populated or de-populated by electrons, without great effects on the MCC stability, because condensation upon oxidation and fragmentation upon reduction is hindered or hampered by the CO shell and the strength of M—M bonds, respectively. In some other cases, e.g. $[Co_8C(CO)_{18}]^{2-}$ [39], $[Co_{13}C_2(CO)_{24}]^{3-}$ [39,55–57] and $[Co_{13}N_2(CO)_{24}]^{3-}$ [57], a synergy arises from the steric pressure exerted by the interstitial main-group element, its strengthening effect on the metal core and the availability of low-lying empty molecular orbitals.
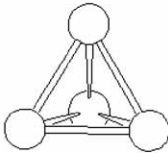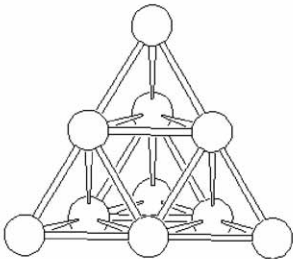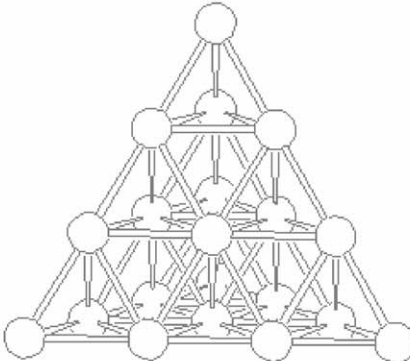
Frequency	ν_1	ν_2	ν_3
Sketch			
CVE	60	132-136	242-254
Δ_{CVE}	0	4	12
Example	$[Fe_4(CO)_{13}]^{2-}$ [24] $Co_4(CO)_{12}$ [25] $Ir_4(CO)_{12}$ [26]	$[Cu_6Fe_4(CO)_{16}]^{2-}$ [27] $[Os_{10}C(CO)_{24}]^{2-}$ [28] $[Ni_7Rh_3(CO)_{18}]^{3-}$ [29]	$[Os_{20}(CO)_{40}]^{2-}$ [30] $[Pd_{16}Ni_4(CO)_{22}(PPh_3)_4]^{2-}$ [31]

Fig. 1. Variation of number of CVE on increasing the frequency ν (as defined by Teo [23]) of a tetrahedral metal geometry [24–31].

The intuition of "ad hoc" conditions such as the above, and the tailored synthesis of MCC which could put them in practice, is often a time-consuming task. It would be much more desirable to have a strategy to induce electron-sink behaviour in MCC or, at least, some guidelines to follow. Probably, the first hint of a possible strategy to override the close-shell configuration of MCC has been provided by complementary works carried out in L.F. Dahl and our laboratories on E-centred Ni_{12} and non-centred

or Ni-centred $Ni_{10}E_2$ (E = post-transition element or molecular moiety) icosahedral carbonyl clusters. As a result of these investigations, E-centred (Fig. 2a) $[Ni_{12}(\mu_{12}\text{-}E)(CO)_{22}]^{2-}$ (E = Ge, Sn) [59], non-centred (Fig. 2b) $[Ni_{10}(\mu_5\text{-}ER)_2(CO)_{18}]^{2-}$ (E = P, As, Sb, Bi; R = alkyl or aryl substituent) [60–66] and Ni-centred (Fig. 2c) $[Ni_{10}(\mu_6\text{-}E)_2(\mu_{12}\text{-}Ni)(CO)_{18}]^{n-}$ (E = Sb, Bi, Se, SnR, Sb → Ni(CO)$_3$) [67–72] derivatives were made available. The E-centred Ni_{12} and non-centred $Ni_{10}E_2$ icosahedral nickel clus-

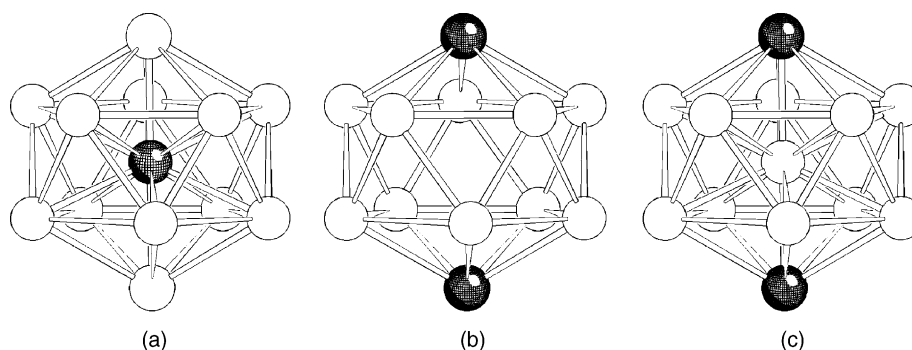
Fig. 2. Schematic representation of the structures of E-centred (a) $[Ni_{12}(\mu_{12}\text{-}E)(CO)_{22}]^{2-}$, non-centred (b) $[Ni_{10}(\mu_5\text{-}ER)_2(CO)_{18}]^{2-}$ and Ni-centred (c) $[Ni_{10}(\mu_6\text{-}E)_2(\mu_{12}\text{-}Ni)(CO)_{18}]^{2-}$ clusters (E atoms are shown as hatched spheres).

ters display conventional electron counts and only exhibit irreversible redox behaviour. In contrast, the Ni-centred $Ni_{10}E_2$ species show anomalous numbers of CVE (8–10 additional electrons with respect to the E-centred and non-centred congeners), reversible electrochemical redox behaviour and multivalence [67–72].

EHMO analysis of $Ni_{10}E_2(\mu_{12}-M)(CO)_{18}$ model compounds with different interstitial M atoms pointed out that, when M = Ni, the out-of-phase combinations of the five d AOs of the interstitial atom with the suitable MO of the $Ni_{10}E_2$ cage are not sufficiently destabilised and fall in the frontier, rather than the antibonding region [68]. This result suggested that interstitial metal atoms, at difference from interstitial main-group elements [73], do not necessarily behave simply as an internal source of electrons, but may alter the number of cluster valence molecular orbitals as a function of the relative energies of their valence atomic orbitals. The presence of these additional weakly antibonding orbitals within or close to the HOMO–LUMO gap increases, perhaps artificially, the electron count. Their redox aptitude is likely triggered by the nature of frontier orbitals, whereas the strengthening effect of the μ_6-E moieties favours the occurrence of multivalence.

Similar conclusions stem from analysis of non-centred $M_8(\mu_4-E)_6L_8$ (M = Fe, Co, Ni; E = S, Se, PPh; L = CO, PR$_3$, Cl, Br, I, SR) and M-centred $M_8(\mu_4-E)_6(\mu_8-M)L_8$ (M = Ni, Pd; E = GeEt, P, As, Sb, Bi; L = CO, PR$_3$) hexacapped cubic clusters [74]. The Ni- and Pd-centred clusters exhibit miscellaneous electron counts in the 121–130 CVE range, while those of non-centred species are comprised in the 99–120 range. Their miscellaneous CVE have been rationalised by EH, DFT and Xα calculations, which pointed out the relevance of both E and L π-donor or π-acceptor properties in determining the electron count within each series. However, the observation that Ni- and Pd-centred clusters are systematically more electron-rich than the non-centred clusters leads once again to conclude that the inclusion principle [73], so nicely effective with interstitial main-group elements, is no more so effectively operative

when the interstitial atom is a late transition element. Interestingly, several of the above clusters display open-shell electronic configurations but, unfortunately, their redox aptitude has only received occasional attention [74].

Perhaps, the best example of the influence of the interstitial atom in affecting the number of CVE is provided by the isostructural series of compounds with formula $[Rh_{13}(\mu_8-Rh)(CO)_{25}]^{4-}$, $[Rh_{13}(\mu_8-Ni)(CO)_{25}]^{5-}$, $[Rh_{12}Ni(\mu_8-Ni)(CO)_{25}]^{4-}$ and $[Rh_9Ni_4(\mu_8-Ni)(CO)_{25}]^{4-}$ [75,76]. The bimetallic Ni–Rh clusters formally derive from replacement with Ni of the interstitial Rh atom in the body-centred cubic structure of the $[Rh_{14}(CO)_{25}]^{4-}$ cluster [75]. The attempt to replace a Rh interstitial atom with Ni in the architecture of the latter MCC could appear awkward, since Ni has a lower heat of atomisation than Rh and the Ni–CO bond is energetic. A "vis-a-vis" comparison of the structures of $[Rh_{13}(\mu_8-Rh)(CO)_{25}]^{4-}$ and $[Rh_{13}(\mu_8-Ni)(CO)_{25}]^{5-}$ is reported in Fig. 3. The major difference between the two is represented by a significant shortening of the four vertical edges of the cubic moiety of $[Rh_{13}(\mu_8-Ni)(CO)_{25}]^{5-}$. It seems, therefore, conceivable to think that the hypothetical $Rh_{12}Ni(\mu_8-Rh) \leftrightarrows Rh_{13}(\mu_8-Ni)$ isomerisation equilibrium is shift to the right, owing to contraction of the Ni-centred Rh_8 cube and the consequent gain of the energy of four extra Rh–Rh interactions. Quite similar reasons are likely at the origin of the successful synthesis of a hexacapped body-centred cubic $[Rh_{14}Ni(CO)_{28}]^{4-}$ derivative [77], whose metal frame is closely related to that of $[Rh_{15}(CO)_{30}]^{3-}$ [78]. Notice that replacement of an interstitial Rh with a Ni atom in all above clusters brings about only a small variation of the number of CVE, in comparison with those (8–10 CVE) triggered by interstitial occupation of an empty icosahedral cluster cage. Thus, the pentacapped Ni-centred cubic Ni–Rh clusters feature 2–4 additional CVE with respect to the Rh-centred $[Rh_{14}(CO)_{25}]^{4-}$. In contrast, the Ni/Rh exchange in the hexacapped body-centred cubic architecture documented by the structure of $[Rh_{14}Ni(CO)_{28}]^{4-}$ seems to correspond to a requirement of two CVE less with respect to
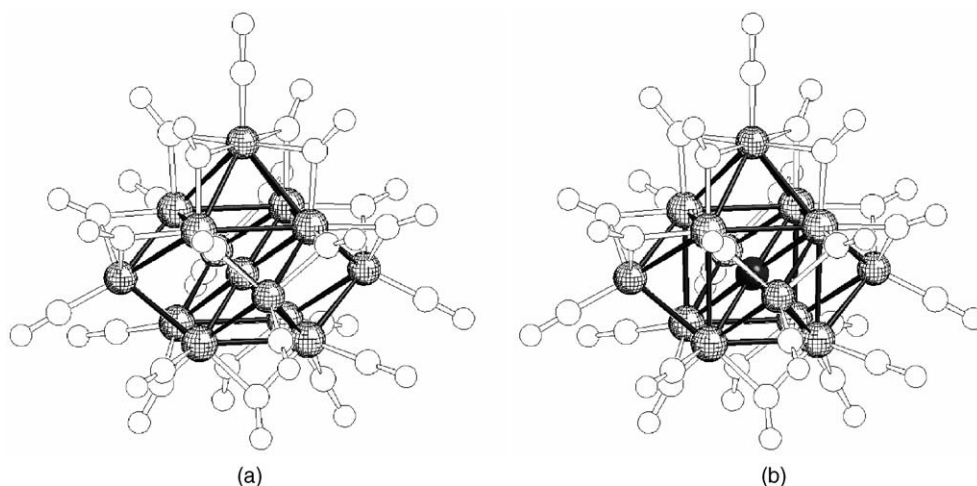

Fig. 3. Vis-a-vis comparison between the structures of $[Rh_{13}(\mu_8-Rh)(CO)_{25}]^{4-}$ (a) and $[Rh_{13}(\mu_8-Ni)(CO)_{25}]^{5-}$ (b): Rh–Rh contacts exceeding the value of 3.0 Å are omitted from both drawings to emphasise differences in the metal frameworks of the two compounds (Ni atom is shown as a blackened sphere; rhodium atoms as hatched spheres).
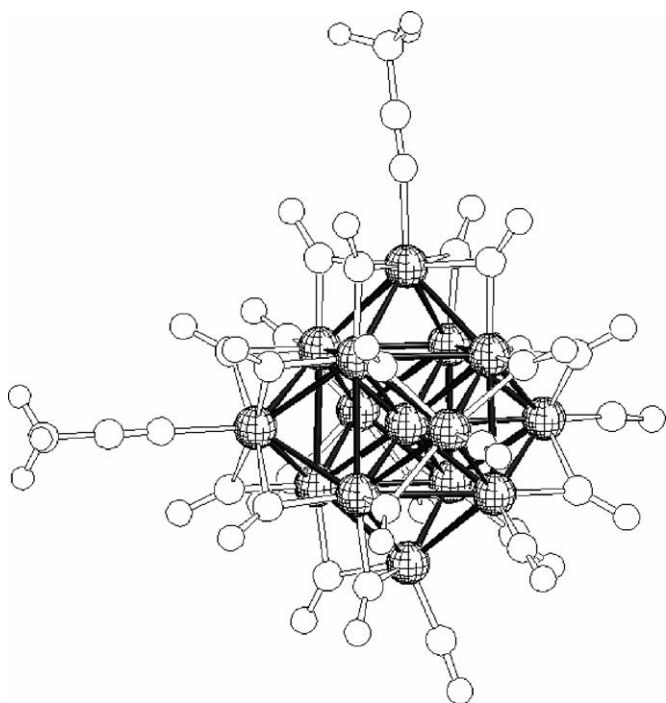
Fig. 4. The structure of the carbonyl-substituted $[Rh_{15}(CO)_{25}(CH_3CN)_2]^{3-}$ tri-anion.

$[Rh_{15}(CO)_{30}]^{3-}$ and two extra CVE in comparison with the carbonyl-substituted $[Rh_{15}(CO)_{25}(CH_3CN)_2]^{3-}$ [79], which displays a likewise regular body-centred cubic metal skeleton (Fig. 4). Interestingly, this latter compound is not isostructural with the isoelectronic homoleptic $[Rh_{15}(CO)_{27}]^{3-}$ cluster [80]. This confirms that the metal frameworks of MCC are rather soft. Their geometry may be affected not only by variations in the number of CVE, but also by the number of peripheral carbonyl groups, as well as the bonding properties of ligands replacing carbonyl groups.

Investigations in progress indicate that the homometallic $[Rh_{14}(CO)_{25}]^{4-}$ only exhibits irreversible redox properties [79]. In contrast, all above Ni-centred tetradecanuclear clusters, perfectly isostructural with $[Rh_{14}(CO)_{25}]^{4-}$, display up to two oxidation and two reduction steps, which show features of chemical reversibility as a function of the solvent. The $[Rh_9Ni_5(CO)_{25}]^{3-}$ cluster is even multivalent. Its corresponding $[Rh_9Ni_5(CO)_{25}]^{2\bullet-}$ odd-electron derivative has been obtained by oxidation of the parent compound with tropylium tetrafluoroborate and structurally characterised [76].

It seems, therefore, possible to conclude that the search for a MCC with nanocapacitor behaviour should be addressed towards clusters containing interstitial metal atoms of late transition elements.

3. Survey of high nuclearity metal carbonyl clusters and carbonyl-substituted metal carbonyl clusters containing interstitial transition-metal atoms

Since the last comprehensive reviews on MCC were published [7–16], the field of MCC has grown to a great extent and the number of species containing at least one interstitial metal atom is now quite large and counts ca. 80 examples, as shown in Table 2. We have included also carbonyl-substituted metal clusters and the coinage metals, being at the border with transition elements. Statistically speaking, all metals belonging to the Groups 9 and 10, as well as the coinage metals, display at least one entry in Table 2. The only notable exception is iridium. The highest nuclearity iridium cluster reported so far is the odd-electron redox-active $[Ir_{14}(CO)_{27}]^-$ species [58]. It only has one electron more than $[Rh_{14}(CO)_{26}]^{2-}$ [86], and in its neutral state is isoelectronic with the latter. Nevertheless, the presence of an additional carbonyl group in the ligand shell causes the adoption of a less round metal framework based on a ν_2-trigonal bipyramid, which does not imply the presence of an interstitial iridium atom. The overwhelming majority of entries of Table 2 regards MCC assembled or containing second and third row elements in either neutral or negative oxidation states. The only apparent exception is the dicationic $[Pd_{14}Au_2(CO)_9(PMe_3)_{11}]^{2+}$ species [111]. The neutral compounds systematically involve efficient σ-donor ligands such as trisubstituted alkyl phosphines.

The panorama disclosed by Table 2 is clearly determined by a few concurrent electronic and steric factors. The prevalence of entries involving second and third row elements is due to the increase of both M–M and M–CO bond energy on descending a group. Peak frequency of MCC for Group 10 metal atom is essentially determined by alleviated steric repulsion between the outer ligands, owing to a decreased need for CVE contributed by the outer ligands. The almost exclusive presence in Table 2 of neutral and anionic species finds an explanation in the π-acidity of carbon monoxide and the relatively high ionisation potentials of some metal atoms (e.g. Pd and Pt), which can be taken as a measure of their propensity to back-donation. Negative charges, or accumulation onto the metal core of a partial negative charge owing to the presence of σ-donor ligands in the MCC coordination sphere, has a beneficial effect on stability of MCC by strengthening M–CO bonds via increased back-donation. Accordingly, the only cationic species, viz. $[Pd_{14}Au_2(CO)_9(PMe_3)_{11}]^{2+}$ [111], displays the highest PR_3/M ratio and involves the rather basic PMe_3 ligand as formal replacement of carbon monoxide.

4. Nanocapacitor behaviour of metal carbonyl clusters

From a formal point of view, a molecular MCC might be considered to be morphologically similar to a macroscopic capacitor. As illustrated in Fig. 5 by the structures of $[Pt_{15}(CO)_{30}]^{2-}$ [137] and $[H_2Ni_{24}Pt_{14}(CO)_{44}]^{4-}$ [128], a MCC is generally based on a kernel of metal atoms surrounded by a shell of carbonyl ligands. Therefore, as a function of the geometry of its metal framework, it might be formally compared with either a cylindrical or spherical metal capacitor. However, before this morphological resemblance could correspond to the above functional property, it is necessary that the MCC fulfils the following requirements.

(1) The MCC should have electron-sink behaviour (in other words, they should be able to reversibly accept and release

Table 2
MCC and carbonyl-substituted MCC containing interstitial metal atoms

N	Compound	Number and kind of interstitial metal atom	Packing	References
Cobalt				
1	$[Co_{11}Te_7(CO)_{10}]^{n-}$ $(n=1, 2)$	1	pp	[81]
2	$Co_{11}Te_7(CO)_5(PMe_2Ph)_5$	1	pp	[81]
Rhodium				
3	$[H_{5-n}Rh_{13}(CO)_{24}]^{n-}$ $(n=2–4)$	1	hcp	[82,83]
4	$[H_{4-n}Rh_{14}(CO)_{25}]^{n-}$ $(n=3–4)$	1	bcc	[75,84]
5	$[Rh_{14}N_2(CO)_{25}]^{2-}$	1	ccp	[85]
6	$[Rh_{14}(CO)_{26}]^{2-}$	1	bcc/hcp	[86]
7	$[Rh_{15}(CO)_{27}]^{3-}$	1	bcc/hcp	[80]
8	$[Rh_{15}(CO)_{25}(CH_3CN)_2]^{3-}$	1	bcc	[79]
9	$[Rh_{15}(CO)_{30}]^{3-}$	1	bcc	[78]
10	$[Rh_{15}C_2(CO)_{28}]^-$	1	pp	[87]
11	$[Rh_{15}C_2(CO)_{24}X_2]^{3-}$ $(X=Cl, Br, I)$	1	pp	[88]
12	$[Rh_{17}(CO)_{30}]^{3-}$	1	hcp	[89]
13	$[Rh_{17}S_2(CO)_{32}]^{3-}$	1	sa	[90]
14	$[Rh_{22}(CO)_{37}]^{4-}$	1	cp	[91]
15	$[H_{8-n}Rh_{22}(CO)_{35}]^{n-}$ $(n=3–6)$	2	bcc	[79,92]
16	$[Rh_{23}N_4(CO)_{38}]^{3-}$	2	irr	[93]
17	$[H_xRh_{28}N_4(CO)_{41}]^{4-}$	3	ccp	[94]
Nickel				
18	$Ni_9(GeEt)_6(CO)_8$	1	bcc	[95]
19	$[NiRh_{13}(CO)_{25}]^{5-}$	1	bcc	[76]
20	$[NiRh_{14}(CO)_{28}]^{4-}$	1	bcc	[77]
21	$[Ni_2Rh_{12}(CO)_{25}]^{4-}$	1	bcc	[76]
22	$[Ni_5Rh_9(CO)_{25}]^{n-}$ $(n=2, 3)$	1	bcc	[76]
23	$[Ni_{10}Te_3(CO)_{15}]^{2-}$	1	ico	[71]
24	$[Ni_{11}Sb_2(CO)_{18}]^{3-}$	1	ico	[69]
25	$[Ni_{11}Bi_2(CO)_{18}]^{3-}$	1	ico	[70]
26	$[Ni_{11}Se_2(CO)_{18}]^{2-}$	1	ico	[71]
27	$[Ni_{11}(SnR)_2(CO)_{18}]^{2-}$ $(R=Me, nBu)$	1	ico	[72]
28	$[Ni_{13}Sb_2(CO)_{24}]^{n-}$ $(n=2, 3)$	1	ico	[67,68]
29	$[Ni_{31}Sb_4(CO)_{40}]^{6-}$	2 (+4 Sb)	ico	[96]
Palladium				
30	$Pd_{16}(CO)_{13}(PMe_3)_9$	1	ico	[97]
31	$Pd_{16}(CO)_{13}(PEt_3)_9$	1	ico	[98]
32	$Pd_{23}(CO)_{22}(PEt_3)_{10}$	1	ccp	[99]
33	$Pd_{23}(CO)_{20}(PEt_3)_{10}$	1	ccp	[100,101]
34	$Pd_{23}(CO)_{20}(PEt_3)_8$	1	bcc	[102]
35	$[Pd_{29}(CO)_{28}(PPh_3)_7]^{2-}$	1	hcp/ccp	[31]
36	$Pd_{30}(CO)_{26}(PEt_3)_{10}$	2	ccp	[105]
37	$Pd_{34}(CO)_{24}(PEt_3)_{12}$		ico	[103]
38	$Pd_{35}(CO)_{23}(PMe_3)_{15}$	5	ico	[97]
39	$Pd_{38}(CO)_{28}(PEt_3)_{12}$	4	irr	[103,104]
40	$Pd_{39}(CO)_{23}(PEt_3)_{16}$	5	ico	[97]
41	$Pd_{54}(CO)_{40}(PEt_3)_{14}$	6	hcp/ccp	[105]
42	$Pd_{59}(CO)_{32}(PMe_3)_{21}$	11	ico	[97,106]
43	$Pd_{69}(CO)_{36}(PEt_3)_{18}$	15	ico	[107]
44	$Pd_{145}(CO)_x(PEt_3)_{30}$	55	ico	[108]
45	$[Pd_8Ni_{36}(CO)_{48}]^{6-}$	6	ccp	[109]
46	$[Pd_{13}Ni_{13}(CO)_{34}]^{4-}$	1	ccp/hcp	[110]
47	$[Pd_{14}Au_2(CO)_9(PMe_3)_{11}]^{2+}$	1	ico	[111]
48	$[Pd_{16}Ni_{16}(CO)_{40}]^{4-}$	2	cp	[112]
49	$[Pd_{20}Ni_{22}(CO)_{46}]^{6-}$	4	cp	[113]
50	$[Pd_{20}Ni_{26}(CO)_{54}]^{6-}$	4	ccp	[112]
51	$Pd_{29}Ni_3(CO)_{22}(PMe_3)_{13}$	4	ico	[97]
52	$[Pd_{33}Ni_9(CO)_{41}(PPh_3)_6]^{4-}$	1	hcp	[31,114]
53	$H_{12}Pd_{28}Pt_{13}(CO)_{27}(PPh_3)_{12}(PMe_3)$	4	hcp	[115]
Platinum				
54	$H_xPt_{15}(CO)_8(PBu^t_3)_6$	1	ccp	[116]
55	$Pt_{17}(CO)_{12}(PEt_3)_8$	1	ico	[117]

Table 2 (*Continued*)

N	Compound	Number and kind of interstitial metal atom	Packing	References
56	$[Pt_{19}(CO)_{22}]^{4-}$	2	pp	[118]
57	$[Pt_{19}(CO)_{21}(NO)]^{3-}$	2	pp	[119]
58	$[Pt_{24}(CO)_{30}]^{2-}$	1	ccp	[120,121]
59	$[Pt_{26}(CO)_{32}]^{2-}$	3	hcp	[121]
60	$[Pt_{38}(CO)_{44}]^{2-}$	6	ccp	[119,121]
61	$[PtRh_{12}(CO)_{24}]^{4-}$	1	hcp	[122]
62	$[Pt_2Rh_{11}(CO)_{24}]^{3-}$	1	hcp	[122]
63	$[Pt_4Rh_{18}(CO)_{35}]^{4-}$	2	bcc	[123]
64	$[Pt_4Ni_{36}(CO)_{45}]^{6-}$	4	ccp	[124,125]
65	$[Pt_4Ni_{37}(CO)_{46}]^{6-}$	4	cp	[124]
66	$[H_{6-n}Pt_6Ni_{38}(CO)_{48}]^{n-}$	6	ccp	[126]
67	$[H_{6-n}Pt_9Ni_{35}(CO)_{48}]^{n-}$	6	ccp	[110]
68	$[Pt_{10}Ni_{14}(CO)_{30}]^{4-}$	2	hcp	[127]
69	$[H_{6-n}Pt_{14}Ni_{24}(CO)_{44}]^{n-}$	6	ccp	[127]
70	$[H_{6-n}Pt_{17}Ni_{24}(CO)_{47}]^{n-}$	6	ccp	[128]
71	$[Pt_{24}Ni_{32}(CO)_{56}]^{n-}$	8	ccp	[128]
Copper				
72	$[Cu_xNi_{35-x}(CO)_{40}]^{5-}$ ($x = 3$ or 5)	3	hcp	[129]
Silver				
73	$[Ag_{13}Fe_8(CO)_{32}]^{n-}$ ($n = 3-5$)	1	ccp	[130–132]
74	$[Ag_{16}Ni_{24}(CO)_{40}]^{4-}$	4	ccp/hcp	[133]
Gold				
75	$[AuPd_{22}(CO)_{20}(PPh_3)_4(PMe_3)_6]^-$	1	ccp	[134]
76	$Au_2Pd_{21}(CO)_{20}(PR_3)_{10}$ (R = Me, Et)	1	ccp	[134]
77	$Au_2Pd_{41}(CO)_{27}(PEt_3)_{15}$	2 (+3 Pd)	ico	[135]
78	$[Au_6Ni_{32}(CO)_{44}]^{6-}$	6	hcp	[136]
79	$[Au_6Pd_6(Pd_{6-x}Ni_x)Ni_{20}(CO)_{44}]^{6-}$ ($x = 2-5.5$)	6	hcp	[136]

bcc = body centred cubic; hcp = hexagonal close packed; ccp = cubic close packed; ico = icosahedral; pp = pentagonal prismatic; cp = complex close packed; sa = square antiprismatic; irr = irregular.

electrons at given potentials while maintaining unaltered their original structures. The MCC should, therefore, be multivalent or, at least, display reversible redox behaviour on the cyclic voltammetry time scale).

(2) The carbonyl ligand shell should effectively insulate the metallic core and hinder or, at least, hamper intermolecular exchange of electrons.

(3) The metallic core of the cluster should undergo transition from insulator-to-metal or be, at least, in a semiconductor regime.

(4) Finally, for practical purposes (see later), the metallic core should display dimensions falling in the nanometric field.

In the following sections we will analyse whether or not MCC fulfil the above four requirements.

4.1. Electron-sink behaviour of metal carbonyl clusters

The findings regarding Ni-centred icosahedral $[Ni_{10}(\mu_{12}-Ni)(\mu_6-E)_2(CO)_{18}]^{n-}$ (E = SnR, Sb, Bi, Se, Te) [67–72] and Ni- or Rh-centred cubic $[Rh_{14-x}Ni_x(CO)_{25}]^{n-}$ ($x = 0-5$) [75,76] clusters suggest that the presence of an interstitial metal atom could be one of the necessary prerequisites in order to systematically observe reversible redox behaviour also in MCC. The electrochemical redox propensity of a considerable number of the clusters reported in Table 2 has been investigated.

The available data are collected in Table 3. Most Co-, Ni-, Pt- and Ag-centred MCC display from two up to six redox changes with features of electrochemical reversibility. In contrast, to our knowledge, both homo- and hetero-metallic Pd-centred clusters only display irreversible reduction and oxidation waves, in spite of the presence of a high number of interstitial Pd atoms. See, for instance, the spectacular $Pd_{145}(CO)_x(PEt_3)_{30}$ cluster, whose metal frame is shown in Fig. 6, which contains 55 interstitial Pd atoms [108]. Particularly indicative in this respect is the behaviour of $[Ni_{36}Pd_8(CO)_{48}]^{6-}$. First of all, this cluster is isoelectronic and isostructural with $[Ni_{38}Pt_6(CO)_{48}]^{6-}$ and $[Ni_{35}Pt_9(CO)_{48}]^{6-}$. Secondly, EHMO calculations point out a similar energy separations of their frontier orbitals. Nevertheless the compound, as well as the related $[Ni_{16}Pd_{16}(CO)_{40}]^{4-}$ [112], $[Ni_{22}Pd_{20}(CO)_{48}]^{6-}$ [113] and $[Ni_{26}Pd_{20}(CO)_{54}]^{6-}$ [112], does not display any interesting redox aptitude and decomposes to yet uncharacterised species. It appears probable that the weakness of all bonds involving palladium could favour large re-arrangements, if not fragmentation or condensation processes, upon reduction or oxidation. That would justify the lack of electron-sink behaviour of several entries of Table 2 involving palladium. A second reason could be the destabilising effect due to the presence of phosphines bearing electron-donor substituents. Indeed, the only anionic species so far reported are $[Pd_{29}(CO)_{28}(PPh_3)_7]^{2-}$ [31] and $[Pd_{33}Ni_9(CO)_{41}(PPh_3)_6]^{4-}$ [31,114], which involve a
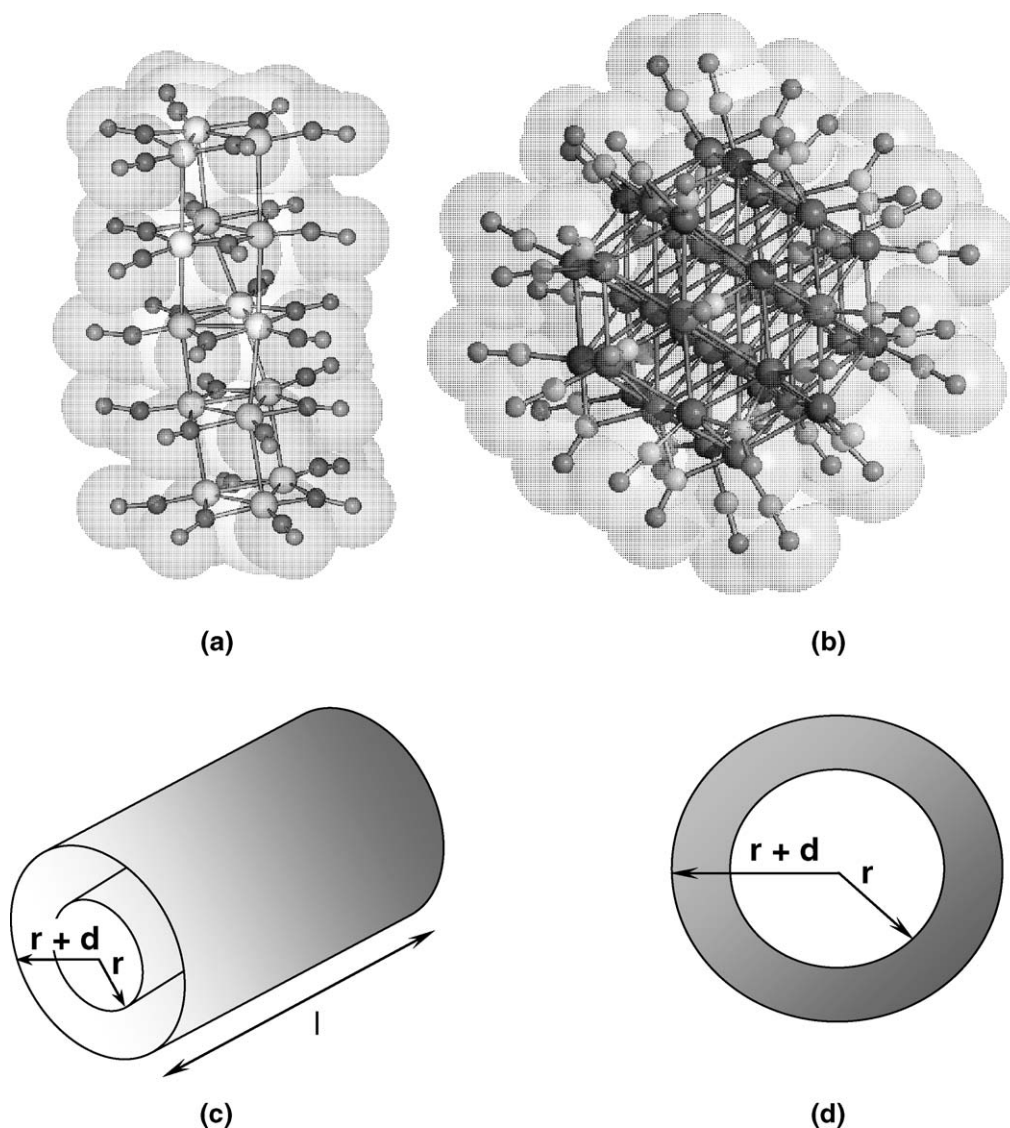
Fig. 5. The structures of $[Pt_{15}(CO)_{30}]^{2-}$ (a) and $[H_2Ni_{24}Pt_{14}(CO)_{44}]^{4-}$ (b) as possible molecular counterparts of cylindrical (c) and spherical (d) capacitors, respectively.

phosphine bearing electron-withdrawing, rather than electron-donor substituents. The first purported factor would suggest that a sufficient robustness of the ligand-stabilised metal cluster is of fundamental importance for observing and, eventually, synthesizing new MCC with nanocapacitor behaviour. At this regard, particularly enlightening examples are $[Co_{11}Te_7(CO)_{10-x}(PMe_2Ph)_x]^{n-}$ ($x=0$, $n=1$; $x=5$, $n=0$) [81] and the $[Ni_{32}C_6(CO)_{36}]^{6-}$ or $[Ni_{38}C_6(CO)_{42}]^{6-}$ carbide clusters. Their metal frameworks are strengthened by the presence of seven capping Te atoms and six interstitial μ_8-C atoms, respectively. As a result, they exhibit among the most notable electron-sink behaviour [81,138]. Strictly speaking there are no interstitial nickel atoms (see Fig. 7) in the above nickel carbide compounds. However, the eight nickel atoms describing the inner cube of $[Ni_{32}C_6(CO)_{36}]^{6-}$ are 12-coordinated (9 Ni + 3 carbide atoms), whereas in $[Ni_{38}C_6(CO)_{42}]^{6-}$ six out of the above eight Ni atoms increase their coordination up to 13

(10 Ni + 3 carbide atoms) [142,143]. It is important to note that the cyclic and hydrodynamic voltammetry of $[Ni_{32}C_6(CO)_{36}]^{6-}$ in acetonitrile solution, reported in Fig. 7, is in perfect agreement with the representation of the frontier energy levels of the cluster pointed out by EHMO calculations with CACAO [144]. Observation of four reduction steps up to $[Ni_{32}C_6(CO)_{36}]^{10-}$ appears to be a direct consequence of filling all energy levels below a small but sufficiently defined energy gap of ca. 0.5 eV. The first two reduction products, viz. the $[Ni_{32}C_6(CO)_{36}]^{7-}$ and $[Ni_{32}C_6(CO)_{36}]^{8-}$ anions, are also readily available upon chemical reduction with sodium-naphthalenide in dimethylformamide and appear to be stable in solution for several hours.

The M–M bond energies of Group 10 bulk metals follow the trend Pd–Pd < Ni–Ni < Pt–Pt. As inferable from chemisorption experiments, as well as calculations on small clusters in gas phase [145–150], M–CO bond energies show an analogous trend (Pd–CO < Ni–CO < Pt–CO). Therefore, platinum-derived

Table 3
Formal redox potentials referred to SCE of redox active MCC containing interstitial metal atoms

	Compound	$E^{\circ\prime}$											References
		+1/0	0/−1	−1/−2	−2/−3	−3/−4	−4/−5	−5/−6	−6/−7	−7/−8	−8/−9	−9/−10	
1	[Co$_{11}$Te$_7$(CO)$_{10}$]$^-$		+0.33	−0.32	−1.04								[81]
2	Co$_{11}$Te$_7$(CO)$_5$L$_5$	−0.08	−0.74	−1.36	−1.90								[81]
3	[HRh$_{14}$(CO)$_{25}$]$^{3-}$			+0.30	−0.20	−1.20	−1.60						[79]
4	[Ni$_{11}$(SnBu)$_2$(CO)$_{18}$]$^{2-}$			−0.25	−1.18								[72]
5	[Ni$_{11}$Sb$_2$(CO)$_{18}$]$^{3-}$			−0.65	−1.42								[69]
6	[Ni$_{11}$Bi$_2$(CO)$_{18}$]$^{3-}$			−0.67	−1.42								[70]
7	[Ni$_{11}$(Sb → Ni(CO)$_3$)$_2$(CO)$_{18}$]$^{3-}$			−0.56	−1.28								[68]
8	[Ni$_5$Rh$_9$(CO)$_{25}$]$^{3-}$			−0.18	−0.35	−1.25							[76]
9	[Ni$_{32}$C$_6$(CO)$_{36}$]$^{6-}$							−0.45	−0.77	−1.06	−1.33	−1.60	[138]
10	[Ni$_{38}$C$_6$(CO)$_{42}$]$^{6-}$							−0.49	−0.98	−1.33	−1.73		[138]
11	[HNi$_{38}$C$_6$(CO)$_{42}$]$^{5-}$							−0.60	−1.11	−1.42	−1.77		[138]
12	[Pt$_{19}$(CO)$_{22}$]$^{4-}$				0.0	−0.31	−1.08	−1.20	−1.93	−2.05			[39]
13	[Pt$_{24}$(CO)$_{30}$]$^{2-}$		+0.64	+0.39	−0.43	−0.69	−1.18	−1.44					[139]
14	[HNi$_{24}$Pt$_{14}$(CO)$_{44}$]$^{5-}$						−0.30	−0.63	−1.11	−1.49			[140]
15	[Ni$_{36}$Pt$_4$(CO)$_{46}$]$^{6-}$							−0.80	−1.15	−1.46	−1.82		[125]
16	[HNi$_{36}$Pt$_4$(CO)$_{46}$]$^{5-}$						−0.70	−1.08	−1.38	−1.76			[125]
17	[Ni$_{38}$Pt$_6$(CO)$_{48}$]$^{6-}$							−0.62	−0.97	−1.29	−1.54	−1.75	[141]
18	[HNi$_{38}$Pt$_6$(CO)$_{48}$]$^{5-}$					−0.25	−0.62	−0.96	−1.28	−1.62			[141]
19	[Ni$_{35}$Pt$_9$(CO)$_{48}$]$^{6-}$						−0.23	−0.63	−1.03	−1.43			[110]
20	[HNi$_{35}$Pt$_9$(CO)$_{48}$]$^{5-}$					−0.30	−0.73	−1.17	−1.38				[110]
21	[Ag$_{13}$Fe$_8$(CO)$_{32}$]$^{3-}$					−0.37	−0.65						[131]

Literature values referred to Ag electrode have been reset to SCE.
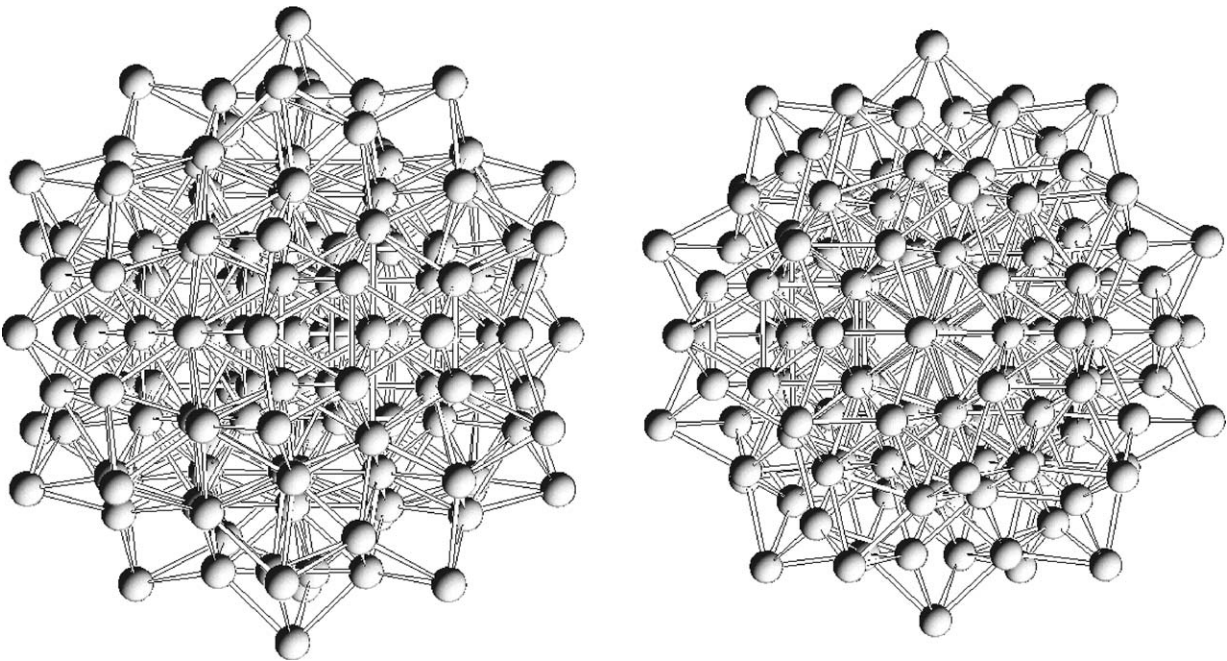
Fig. 6. Two orthogonal views of the Pd$_{145}$(CO)$_x$(PEt$_3$)$_{30}$ metal frame of Pd$_{145}$ [108].

MCC are expected to be the most robust of the Group. Accordingly, both homo- and hetero-metallic Pt clusters containing interstitial Pt atoms show the most remarkable reversible redox properties. For instance, [Pt$_{19}$(CO)$_{22}$]$^{4-}$ and [Pt$_{24}$(CO)$_{30}$]$^{2-}$ show several redox waves with features of electrochemical reversibility [39,139,151]. Their cyclic voltammetric profiles show features which are displayed also by other redox-active low-nuclearity MCC: pairs of closer redox waves separated by larger gaps [39]. The staircase-like trend of z-plots (z is the charge of the most reduced species involved in the redox couple) versus the formal redox potentials of [Pt$_{19}$(CO)$_{22}$]$^{2-}$, [Pt$_{24}$(CO)$_{30}$]$^{2-}$ and [HRh$_{14}$(CO)$_{25}$]$^{2-}$ is illustrated in Fig. 8, as an example. Moreover, the gap between the pairs of redox waves decreases as the MCC nuclearity increases (compare,
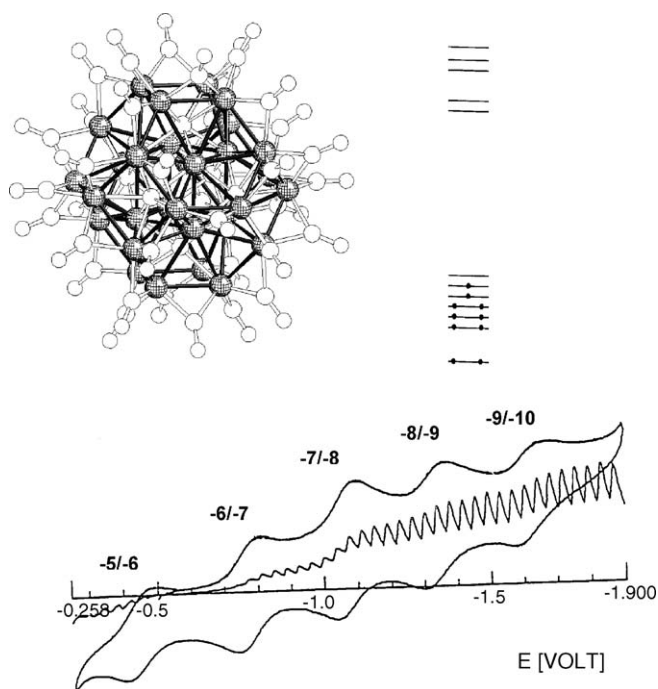
Fig. 7. The structure, the cyclic voltammetric profile and the EHMO frontier region of $[Ni_{32}C_6(CO)_{36}]^{6-}$.

for instance, $E^{\circ\prime}_{-2/-3} - E^{\circ\prime}_{-3/-4}$ of $[HRh_{14}(CO)_{25}]^{z-}$ with $E^{\circ\prime}_{-4/-5} - E^{\circ\prime}_{-5/-6}$ of $[Pt_{19}(CO)_{22}]^{z-}$ in Fig. 8). It seems reasonable to conclude that electrons enter in pairs by first semi-occupying and then filling one-by-one the frontier molecular orbitals, owing to the presence of discrete levels with an energy separation yet superior to the pairing energy.

In contrast, the cyclic voltammetric profile of higher-nuclearity MCC, such as $[H_{6-n}Ni_{36}Pt_4(CO)_{46}]^{n-}$ [125] and $[H_{6-n}Ni_{38}Pt_6(CO)_{48}]^{n-}$ [141], which respectively contain four and six interstitial platinum atoms, displays almost equally spaced redox waves. These correspond to one oxidation and up to four reduction steps with features of reversibility on the
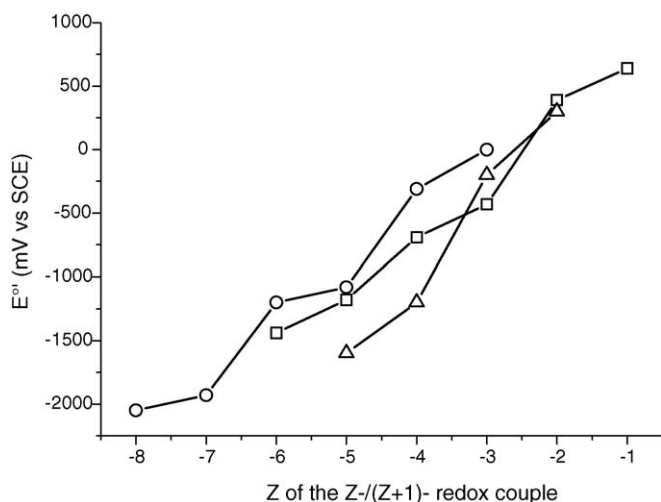

Fig. 8. Staircase-like z-plots of the formal redox potentials ($E^{\circ\prime}$ vs. SCE) of $[Pt_{19}(CO)_{22}]^{z-}$ (○), $[Pt_{24}(CO)_{30}]^{z-}$ (□) and $[HRh_{14}(CO)_{25}]^{z-}$ (△).
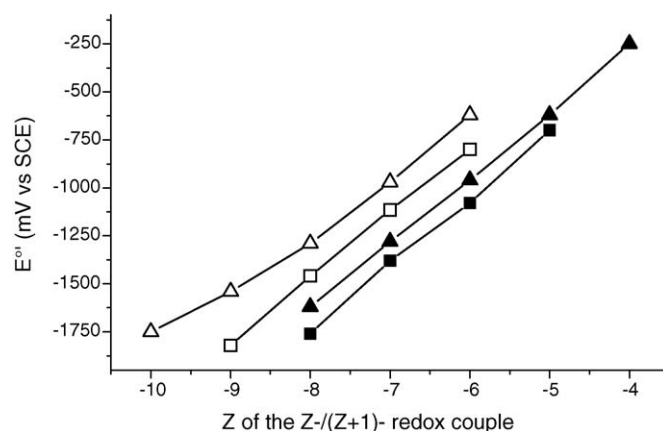

Fig. 9. Linear trend of z-plots vs. formal redox potentials ($E^{\circ\prime}$ vs. SCE) of $[Ni_{36}Pt_4(CO)_{45}]^{z-}$ (□), $[HNi_{36}Pt_4(CO)_{45}]^{z-}$ (■), $[Ni_{38}Pt_6(CO)_{48}]^{z-}$ (△) and $[HNi_{38}Pt_6(CO)_{48}]^{z-}$ (▲).

cyclic voltammetric time scale. As a result, the plots of their formal potentials versus the charge z of the most reduced species involved in the redox couple display an almost perfect linear fit (see Fig. 9).

The electron-sink properties of the above clusters are somehow contrasted by the behaviour of $[Pt_{26}(CO)_{32}]^{2-}$ and $[Pt_{38}(CO)_{44}]^{2-}$ [39,139,151], which respectively contain three and six interstitial Pt atoms; spectroelectrochemical experiments did disclose a rich redox chemistry. However, by visual inspection, some redox changes seem to involve more than one electron and some others seem to be electrochemically irreversible. Nevertheless, the multivalence of $[Pt_{26}(CO)_{32}]^{2-}$, as well as that of $[Pt_{24}(CO)_{30}]^{2-}$, has been demonstrated beyond any doubt by isolation upon chemical oxidation of their corresponding mono-anionic and neutral derivatives [152]. Notice that $Pt_{24}(CO)_{30}$ and $Pt_{26}(CO)_{32}$ represent the first structurally characterised neutral homoleptic carbonyl derivatives of platinum. The existence of platinum-chloro-carbonyl derivatives and the non-existence of $Pt(CO)_4$ have been respectively related to the relatively high electron affinity and ionisation potential of Pt in a d^{10} electronic configuration [153]. A high electron affinity, further enhanced by a positive oxidation state of Pt, favours σ-donation from CO, whereas reluctance for π-backdonation due to high ionisation potential could be released by clustering, as well as a fractional negative oxidation state of platinum. Accordingly, several platinum carbonyl cationic [154] and anionic species are now known. Besides, it seems conceivable that the existence of neutral $Pt_{24}(CO)_{30}$ and $Pt_{26}(CO)_{32}$ homoleptic carbonyls could be attributed to a clustering effect.

4.1.1. Modulation of electronic properties of metal carbonyl clusters and tuning of their redox potentials

The chemical behaviour of anionic MCC provides some opportunities to modulate their electronic properties and tune the redox potentials of a given cluster. The first documented possibility is provided by the progressive substitution of π-acidic carbonyl groups with stronger σ-donor ligands such as phosphines. The most significant example is undoubtedly the $[Co_{11}Te_7(CO)_{10-x}(PMe_2Ph)_x]^n$ ($x = 0-5$; n ranging from +1 to

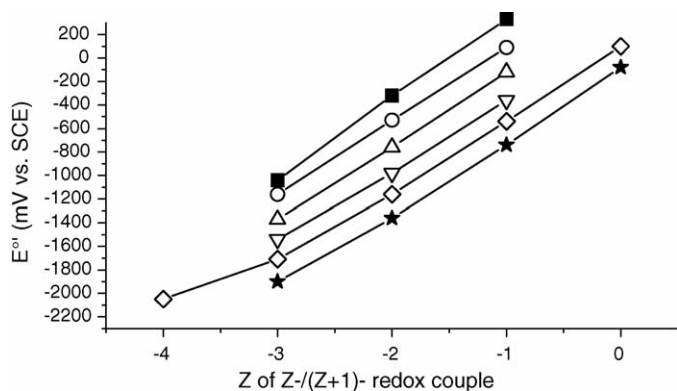Fig. 10. *z*-Plots of $E^{\circ\prime}$ (vs. SCE) of $[Co_{11}Te_7(CO)_{10-x}(PMe_2Ph)_x]^{z-}$ ($(\blacksquare)$ $x = 0$; $(\bigcirc)$ $x = 1$; $(\triangle)$ $x = 2$; $(\triangledown)$ $x = 3$; $(\diamond)$ $x = 4$; $(\star)$ $x = 5$).

−4) family of clusters [81]. Five carbonyl groups of the Co-centred $[Co_{11}Te_7(CO)_{10}]^-$ pentagonal prismatic mono-anion, probably owing to the stabilizing effect of the seven Te caps, can be progressively substituted by dimethylphenylphosphine. As graphically shown in Fig. 10, the consequences of an increasing negative charge residing on the cluster as *x* increases are the following: first of all, correspondent redox changes progressively occur at more negative potentials (ca. −0.2 V per each replacement of a carbon monoxide group by a phosphine ligand). Secondly, the highest oxidation states gain in stability. As a result the most stable species with $x = 5$ is the neutral $Co_{11}Te_7(CO)_5(PMe_2Ph)_5$ species, which has been isolated and structurally characterised [81].

A second possibility can be provided by protonation of a polyanionic cluster. As shown in Table 3 and Fig. 9, formal replacement of a negative charge of the parent polyanion with a hydrogen atom (compare, for instance, the following pairs of entries: 10–11, 15–16, 17–18 and 19–21 in Table 3 or empty and filled square and circle fits in Fig. 9) has two major effects. First of all, occurrence of the same redox change in the hydride derivative requires a more negative potential. That probably follows from the fact that non-hydride and hydride derivatives possessing the same negative charge are not isoelectronic and the latter has one more CVE. Likely as a further consequence of that, hydride derivatives often show a decreased number of reduction and an increased number of oxidation steps. Moreover, a small variation in both $E^{\circ\prime}$ and $\Delta E^{\circ\prime}$ between consecutive redox couples is observed. The occurrence of these effects, beyond other considerations, provides a circumstantial evidence of the presence of hydride atoms in those cases where the direct proof via ^1H NMR could not be obtained. However substitution of negative charges with hydrogen atoms can have several other contrasting consequences, besides tuning the redox potentials of a given cluster via modulation of its electronic properties. On one hand, it can also induce redox aptitude in an otherwise redox inactive cluster. This is the case of the $[HRh_{14}(CO)_{25}]^{3-}$ and $[Rh_{14}(CO)_{25}]^{4-}$ pair of compounds [79]. As already mentioned, the latter does not display any meaningful reversible voltammetric feature. In contrast, as inferable from Fig. 8, the former shows two oxidation and two reduction waves which achieve features of chemical reversibility as a function of the sol-

vent. On the other hand, the presence of more than one hydride atom can be detrimental for electron-sink behaviour. This is the case for instance of $[H_{5-n}Rh_{13}(CO)_{24}]^{n-}$ ($n = 2$ and 3) and $[H_{6-n}Ni_{38}Pt_6(CO)_{48}]^{n-}$ ($n = 4$). These compounds only show either one or two redox changes with features of electrochemical reversibility, probably owing to easy reductive elimination of hydrogen molecules.

A third way to modulate the electronic properties and tune the redox potentials of a given cluster is replacing some surface metal atoms with a different transition metal atom. Possible examples of this opportunity are the already mentioned $[Ni_{13-x}Rh_x(\mu_{12}\text{-}Ni)(CO)_{25}]^{n-}$ ($x = 13$, 12, 9) [76], and also the high nuclearity $[Ni_{38-x}Pt_x(CO)_{44}]^{n-}$ ($x = 38$, 14) [39,121,140] and $[Ni_{44-x}Pt_x(CO)_{48}]^{n-}$ ($x = 6$, 9) clusters [109,141]. As shown, for instance, by a comparison between entries 17–19 and 18–20 of Table 3, replacing three Ni with three Pt atoms on the surface of $[Ni_{38}Pt_6(CO)_{48}]^{6-}$ has a series of consequences. First of all, the presence of three Pt atoms in place of Ni onto the surface of the cluster shifts to more negative potentials the corresponding redox changes. It seems reasonable to suggest that this effect could be due to a higher residual negative charge onto the metal core, owing to a decreased back-donation onto the carbonyl groups. This suggestion is supported by comparison of the infrared spectra of $[H_{6-n}Ni_{35}Pt_9(CO)_{48}]^{n-}$ and $[H_{6-n}Ni_{38}Pt_6(CO)_{48}]^{n-}$. The pattern is identical but the absorptions of both terminal and bridging carbonyl groups of the former are correspondingly shifted to higher wavenumbers (5–10 cm^{-1}) than in the latter. Meanwhile, an increased amount of Pt in the cluster seems to decrease the number of reversible reduction steps and favours the occurrence of more oxidized redox changes. After all, this is in keeping with the stability and isolation of the high-nuclearity neutral homoleptic Pt carbonyls mentioned before.

The opposite example, replacement of Pt with Ni, is illustrated by a comparison of the two quasi-isostructural $[Pt_{38}(CO)_{44}]^{2-}$ and $[H_2Ni_{24}Pt_{14}(CO)_{44}]^{4-}$ MCC. The two only differ in the carbonyl stereochemistry: $[Pt_{38}(CO)_{44}]^{2-}$ has four more terminal and four less edge-bridging carbonyl groups than $[H_2Ni_{24}Pt_{14}(CO)_{44}]^{4-}$. The effect of replacing metal atoms is shown in Fig. 11, which illustrates the frontier region of the MO diagram of $[Pt_{38}(CO)_{44}]^{2-}$ and the $[Ni_{24}Pt_{14}(CO)_{44}]^{4-}$ moiety of $[H_2Ni_{24}Pt_{14}(CO)_{44}]^{4-}$, as well as the voltammetric response of $[HNi_{24}Pt_{14}(CO)_{44}]^{5-}$. As suggested by EHMO calculations both $[Pt_{38}(CO)_{44}]^{n-}$ and $[Ni_{24}Pt_{14}(CO)_{44}]^{n-}$ non-hydride moieties might be expected to withstand a charge comprised in the range +2 and −10. Both MO diagrams point out the presence of six tightly spaced MOs within a wider energy gap. Partially in keeping with this suggestion, the parent $[HNi_{24}Pt_{14}(CO)_{44}]^{5-}$ can be reversibly reduced down to $[HNi_{24}Pt_{14}(CO)_{44}]^{8-}$ (see Fig. 11 on the right).

As a final remark in this section, it seems justified to conclude that MCC containing interstitial late-transition metal atoms fulfil the first requirement in order to be compared with molecular capacitors. From a formal point of view, the voltammetric profiles of several MCC are strictly comparable with those exhibited by C_{60} [155] and quasi-molecular gold particles stabilised in thiol shells [156–159].
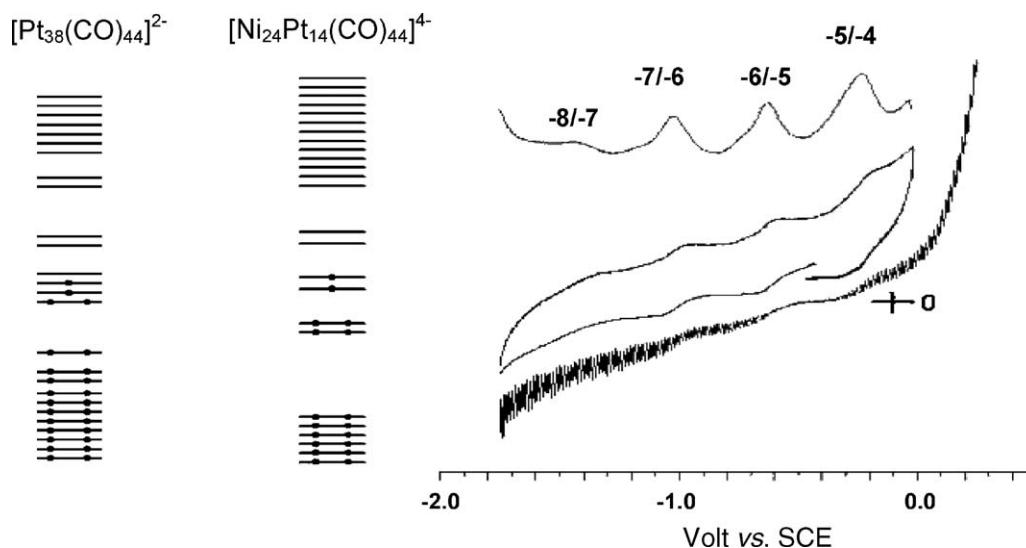
Fig. 11. Comparison between the frontier regions between −11 and −9.5 eV of $[Pt_{38}(CO)_{44}]^{2-}$ and the $[Ni_{24}Pt_{14}(CO)_{44}]^{4-}$ moiety of $[H_2Ni_{24}Pt_{14}(CO)_{44}]^{4-}$ (left) and differential pulse, cyclic voltammetry and hydrodynamic behaviour of $[HNi_{24}Pt_{14}(CO)_{44}]^{5-}$ (right).

4.2. The effectiveness of the CO shielding

The importance of the second requirement stems from the consideration that easy intermolecular exchange of electrons in solution, which could possibly take place also in the solid state, would hinder effective storage of electrons in the MCC molecule. Coulombic repulsion might generate an energy barrier for intermolecular exchange of electrons also in ligand-free post-transition metal clusters, e.g. M_9^{n-} (M = Ge, Sn, Pb; $n = 3$ and 4) Zintl ions [160,161], C_{60}^{n-} fullerides [162], and their endohedral derivatives [163,164]. However, at least in the case of C_{60}^{n-} fullerides, the Coulombic energy barrier is not sufficient to hinder intermolecular electron exchange in solution, which is fast on the time scale of ^{13}C NMR. Indeed, mixtures of differently charged fullerides, e.g. C_{60}/C_{60}^- and C_{60}^{2-}/C_{60}^{3-}, display ^{13}C NMR chemical shifts intermediate between the values of their respective pure anions [162]. Moreover, exchange of electrons in the solid state cannot be ruled out. In the case of Zintl ions, further complications arise, owing to occurrence of oxidative coupling. For instance, oxidation of $[Ge_9]^{4-}$ can lead to $[Ge_9]^{n-}$ ($n = 3$ and 2) clusters, $[(Ge_9)_2]^{6-}$ and $[(Ge_9)_n]^{2n-}$ ($n = 3$ and 4) oligomers and the zigzag chain $\{[Ge_9]^{2-}\}_\infty$ polymer [163,164], as a function of reaction procedures.

Although the effectiveness of the carbonyl shielding in the long run is yet unknown, EPR experiments suggest that intermolecular electron exchange between differently charged MCC is not fast. Indeed, the EPR patterns of the odd-electron $[Fe_3Pt_3(CO)_{15}]^-$ and $[Ag_{13}Fe_8(CO)_{32}]^{4-}$ are unaffected by the presence of their respective even-electron $[Fe_3Pt_3(CO)_{15}]^{0/2-}$ and $[Ag_{13}Fe_8(CO)_{32}]^{3-/5-}$ congeners at all ratios and temperatures, both in solution and in the solid state. Notice that owing to coupling of the unpaired electron with ^{195}Pt and ^{107}Ag–^{109}Ag, respectively, the hyperfine structure of the EPR spectra of $[Fe_3Pt_3(CO)_{15}]^-$ and $[Ag_{13}Fe_8(CO)_{32}]^{4-}$ is an unambiguous fingerprint. Should intermolecular electron exchange between differently charged species be fast on EPR time scale,

the coupling with spin active nuclei would have been affected. The metal core of MCC behaves, therefore, as a quantum dot in which electrons are confined [132,165,166].

4.3. Size-induced insulator-to-metal transition of the metal core of metal carbonyl clusters

As partially anticipated in Section 4.1, the voltammetric profiles of the redox-active carbonyl clusters change as a function of nuclearity. Typical profiles of low-nuclearity clusters with extensive redox aptitude are represented by those of $[HRh_{14}(CO)_{25}]^{3-}$, $[Pt_{19}(CO)_{22}]^{4-}$ or $[Pt_{24}(CO)_{30}]^{2-}$ (see z-plots in Fig. 8). The difference with that of a higher-nuclearity cluster, as exemplified by that of $[Ni_{32}C_6(CO)_{36}]^{6-}$, reported in Fig. 7, or the z-plots of $[H_{6-n}Ni_{36}Pt_4(CO)_{46}]^{z-}$ and $[H_{6-n}Ni_{38}Pt_6(CO)_{48}]^{z-}$ ($n = 0$ and 1) of Fig. 9, is rather evident. The former is suggestive of a close-shell cluster displaying a rather wide HOMO–LUMO gap of ca. 1.5 eV (as inferable from the difference in Volts between the formal redox potentials of the $[HRh_{14}(CO)_{25}]^{3-/4-}$ and $[HRh_{14}(CO)_{25}]^{4-/5-}$ pairs) and a pairing energy of ca. 0.3 eV in the related orbitals. The latter might be due to an open-, as well as a close-shell cluster, and the interpretation of the spacing may change in consequence. In any case, the average separations between the formal electrode potentials of consecutive redox couples of MCC displaying multiple reversible redox changes decrease as a function of the nuclearity. Indeed, the consecutive one-electron transitions progressively become almost equally spaced and tight as the nuclearity of the cluster increases. Average ΔEs down to 0.25–0.3 V have been observed (see Table 3). Miscellaneous plots of average ΔE versus nuclearity (abscissa) for different collections of MCC display satisfactory linear fits with correlation coefficients up to a ca. 99% level, in spite of the dispersion of the ΔE between consecutive redox couples and almost independently from the MCC composition. All plots agree in showing extrapolated intercepts at ca. 0.75 V in ordinate and 65–70 in abscissa [141]. An exam-
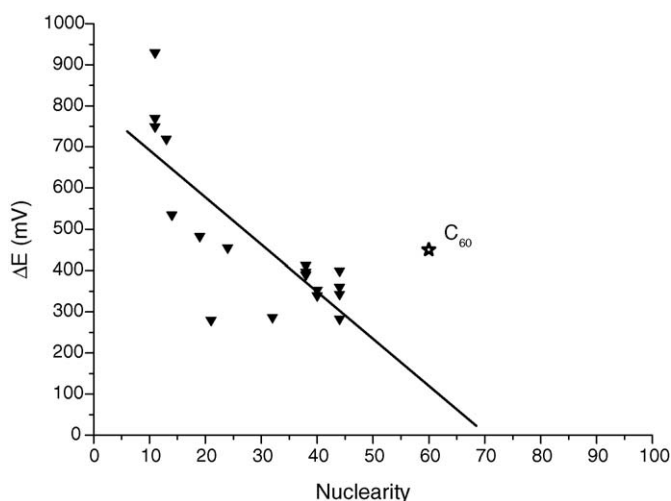
Fig. 12. Experimental average separation of consecutive redox couples (ΔE_{av} in V) as a function of the nuclearity of the cluster. Entries represented by filled triangles are due to MCC collected in Table 3, while the star represents the average ΔE displayed by the consecutive redox couples of C_{60} [162].

ple of such plots is given in Fig. 12. It includes all entries of Table 3 and, consequently, the linear fit displays a low correlation coefficient. For sake of comparison, the entry relative to $[C_{60}]^{n-}$ has also been included.

A first consideration suggested by Fig. 12 is that isolation of redox-active MCC beyond a nuclearity of ca. 60–65 could be hampered by occurrence of significant disproportionation equilibria in solution. Indeed, if the linear fitting holds beyond the last experimental entry, the extrapolated values of ΔE decreases to ca. 0.06 V in the above range of nuclearities. Therefore, the constant of a disproportionation equilibrium such as (1) could assume values close to 0.1 and greater than that.

$$2[MCC]^n \leftrightarrows [MCC]^{n-1} + [MCC]^{n+1} \qquad (1)$$

On the other side, the separations between formal electrode potentials of consecutive redox couples (ΔE) substantially mirrors the differences between their ionisation energies. Therefore, these ΔE may be extrapolated to approximately quantify the energy separation in eV between the frontier one-electron energy levels. Within this premise, the present one-electron energy separations suggest that the MCC so far investigated still possess a semiconductor rather than a metal-like nature. However, according to Fig. 12, the size-induced metallisation process of MCC is well underway and the transition could be expected to occur for nuclearities above a likely threshold value of ca. 70. Although such nuclearity has already been reached and exceeded by carbonyl-substituted clusters, e.g. $Pd_{69}(CO)_{36}(PEt_3)_{18}$ [107] and $Pd_{145}(CO)_x(PEt_3)_{30}$ ($x \sim 60$) [108], the above expectation cannot be substantiated because, to our knowledge, their redox behaviour has not been reported yet.

The above conclusion about metallisation of MCC is in satisfactory agreement with the results of other attempts to experimentally determine the size-induced metal–insulator transition of MCC and clusters. First of all, it seems significant that interpretation of the astonishing simplicity of infrared spectra of MCC requires a symmetry-based spherical harmonic model

which may be related to a symmetry-based restatement of the surface selection rules [167]. Secondly, it is rewarding that spectroscopic studies on CO adsorbed on palladium islands deposited on alumina films point out that aggregation of ca. 100 Pd atoms is necessary in order to observe transition from molecular to metallic features [168]. Very similar size regimes have been observed to determine a size-induced metal–insulator transition for bare Hg and Au clusters in gas phase [169]. For instance, photoelectron spectroscopy studies on mass-selected bare Au_n clusters suggest that bulk properties begin to emerge for $n > 40$ [170]. Accordingly, a locally resolved scanning tunnelling spectroscopy study at 7 K in precise sites of $Au_{55}(PPh_3)_{12}Cl_6$ suggests a level spacing in proximity of Fermi level of ca. 170 meV [171]. Such a spacing situates $Au_{55}(PPh_3)_{12}Cl_6$ in close proximity of the extrapolated straight line of Fig. 12.

It has, however, to be mentioned that all available data regarding quasi mono-dispersed gold clusters stabilised by a protecting monolayer of thiols (MPC) do not conform to the above prediction and would fall far outside the plot of Fig. 12. Indeed, MPC in a purported 140–147 range of nuclearity behave as extremely efficient electron sinks and reservoirs [156–159], but exhibit ΔEs between consecutive redox couples (0.2–0.4 V) of the same order of magnitude of $[Ni_{32}C_6(CO)_{36}]^{6-}$ or $[Ni_{38}Pt_6(CO)_{48}]^{6-}$. It might be a hint that the plot of Fig. 12 will change slope for nuclearities greater than 44 and reach a plateau approximately ranking around ca. 0.2 V. At the present stage, it could be speculated that the yet semiconductor nature of the above gold clusters might mean that their metallisation is slowed down by the thiol (or thiolate) ligands shielding the gold particle or, less likely, by the electronic properties of the gold itself (see above).

4.4. The size of metal carbonyl clusters

The final condition regards the size of MCC. A nanometric size is essential in order to have the possibility to interrogate a single MCC molecule, rather than a collection of molecules, even if perfectly identical to each other. Communication with a single molecule by single electron transfer could allow, for instance, to store a bit of information at molecular level. This last requisite is fulfilled by a good number of so far reported MCC. Several low-valent metal clusters, stabilised mainly or uniquely by carbonyl ligands, besides being molecules or molecular ions perfectly defined in composition and all structural details, trespass by size in the field of nanomaterials (1–1000 nm) from the lowest limit. Pseudo 1D MCC possessing nanometric size have been known for a long time. For instance, the $[Pt_{15}(CO)_{30}]^{2-}$ dianion [137], shown in Fig. 5, has a metal frame length of ca. 1.5 nm. More or less spherical or ellipsoidal clusters, such as $[Ni_{32}Pt_{24}(CO)_{56}]^{6-}$ [128], $[Ni_{26}Pd_{20}(CO)_{54}]^{6-}$ [112], $Pd_{59}(CO)_{32}(PMe_3)_{21}$ [106], $Pd_{69}(CO)_{36}(PEt_3)_{18}$ [107] and the giant three-shell $Pd_{145}(CO)_x(PEt_3)_{30}$ ($x \sim 60$) [108], display metallic core diameters in the 1–2 nm range. In any case, size does not seem to be a serious limitation because of the possibility to aggregate MCC molecules in several ways (see Section 6). Several MCC aggregates close or trespassing in the nanofield can be prepared, for instance by the fusion of two or more anionic clusters with a central core consti-

tuted by a single cation, e.g. $\{Hg[Os_{10}C(CO)_{24}]_2\}^{2-}$ [172], or cationic cluster moieties, e.g. $\{Cd_2Cl_3[Ni_6(CO)_{12}]_2\}^{3-}$ [173], $[H_2Ru_{12}Cu_6Cl_2(CO)_{34}]^{2-}$ [174], $[H_4Ru_{20}Cu_6Cl_2(CO)_{48}]^{4-}$ [175], and $[Ag_3Ru_{10}C_2(CO)_{28}Cl]^{2-}$ [176]. Besides, the existence in solution of several fused MCC moieties such as $\{Ag[Rh_6C(CO)_{15}]_2\}^{3-}$ and higher $\{Ag_{n-1}[Rh_6C(CO)_{15}]_n\}^{n-}$ oligomers has been demonstrated several years ago by multinuclear NMR [177], and envisions the possibility to isolate MCC aggregates well beyond 2 nm.

4.5. Metal carbonyl clusters as molecular nanocapacitors

On the basis of the results described in the previous sections, it seems reasonable to conclude that several MCC reported in Table 3 are truly similar to molecular nanosized capacitors. Indeed:

1. Their metal core is in the semiconductor regime and on the way to undergo a size-induced semiconductor–metal transition.
2. Their dimensions are nanometric (1–2 nm).
3. The surrounding shell of carbonyl ligands probably provides an intermolecular shielding sufficiently efficient to hamper ready electron exchange.
4. The electronic properties of the molecular cluster can be modulated by subtle variation of the metal composition and ligands shell, as well as by involvement of interstitial metal atoms and main-group elements.
5. Their redox potentials are tunable.

The capacitance C of the molecular capacitors reported in Table 3 can be evaluated by Eq. (2),

$$C = \frac{q}{\Delta V} \qquad (2)$$

where q represents the electron charge (1.6×10^{-19} C) and ΔV is the ΔE_{av} reported in Fig. 12. As shown by calculations on a few selected examples reported in Table 4, it turns out that capacitance ranges from 0.2 to 0.6 aF per molecule and roughly increases as a function of MCC nuclearity and size.

The capacitance of a spherical metal capacitor ($C_{s.m.c.}$), such as that depicted in Fig. 5, depends from its radius and the thickness of the dielectric layer, according to Eq. (3), where ε_o is the

dielectric constant of vacuum (8.85×10^{-12} F/m),

$$C_{s.m.c.} = \frac{4\pi\varepsilon_o\varepsilon r(r+d)}{d} \qquad (3)$$

where ε is dielectric constant of the insulator layer (the CO monolayer in the present case), r radius of the metallic sphere and d is the thickness of the dielectric layer. Analogously, the capacitance of a cylindrical metal capacitor ($C_{c.m.c.}$), is given by Eq. (4), where l is the length of the cylinder.

$$C_{c.m.c.} = \frac{2\pi\varepsilon_o\varepsilon l}{\ln((r+d)/r)} \qquad (4)$$

Being known the capacitance C of a given MCC, Eqs. (3) and (4) allow evaluation of the dielectric constant of the CO monolayer. The reliability of calculated $\varepsilon_{CO\,monolayer}$ has the limit that MCC can only be very roughly approximated to cylinders or spheres. The radius of the sphere inscribing the whole MCC metal core (viz. the distance from MCC centre and the centre of farthest metal atom, plus the radius of the peripheral metal atom itself) can be taken as the value of r for spherical metal capacitors, whereas the corresponding distances along the shortest and longest extensions of a cylindrical MCC have been, respectively, taken as r and $1/2l$. In both cases, the thickness d of the CO layer has been evaluated by the following Eq. (5), where d_{b-O} is the distance of the barycentre of MCC and the farthest oxygen atom, r is the radius of the metal core calculated as above and r_O is the covalent radius of oxygen.

$$d = d_{b-O} - r + r_O \qquad (5)$$

As shown in Table 4, calculations on some selected examples of MCC with nuclearity ranging from 11 to 44, which may be reasonably considered as cylindrical or spherical, gave values of $\varepsilon_{CO\,monolayer}$ in the rather narrow 1.6–1.7 range. The value of $\varepsilon_{CO\,monolayer}$ slightly increases to a 2.1–2.2 range by substituting covalent with the van der Waals radius of the oxygen atom in Eq. (5). Both these values are greater than the ε of gaseous (1.003), liquid (ca. 1.5 as inferable from its refraction index at 78 K) and solid carbon monoxide (1.5455 at 29.65 K) [178]. A dielectric constant greater than that of solid carbon monoxide seems reasonable and in keeping with the inherent perfect orientation of CO molecules coordinated through the carbon atom to the MCC. In contrast, the residual entropy of solid CO at 0 K suggests its random orientation in the crystal. To our knowledge, the only available data on the dielectric constant of adsorbed CO are those relative to Cu and Ag films, which are in keeping with the above conclusion [179].

5. Comparison of the nanocapacitor behaviour of metal carbonyl clusters with that of quasi-molecular metal particles stabilised in a ligand shell

Nearly mono-dispersed metal nanoparticles, sized from 1 to 10 nm in diameter, have experienced an increasing interest over the last two decades, owing to the belief that they will show quite unique properties due to quantum size effects. It is believed that these quasi-molecular metal particles hold potential in several

Table 4
Capacitance (C) of cylindrical and spherical MCC and calculated dielectric constant of coordinated carbon monoxide ($\varepsilon_{CO\,monolayer}$)

MCC	C (aF)	r (nm)	d (nm)	l (nm)	$\varepsilon_{CO\,monolayer}$
Cylindrical capacitor					
$[Pt_{19}(CO)_{22}]^{4-}$	0.37	0.40	0.13	1.08	1.7
Spherical capacitor					
$[Ni_{11}Sb_2(CO)_{18}]^{3-}$	0.21	0.38	0.19		1.7
$[HRh_{14}(CO)_{25}]^{3-}$	0.25	0.47	0.23		1.6
$[HNi_{24}Pt_{14}(CO)_{44}]^{5-}$	0.40	0.57	0.19		1.6
$[Ni_{38}Pt_6(CO)_{48}]^{6-}$	0.57	0.67	0.19		1.7

fields going from nanoelectronics to catalysis. Several authoritative reviews and books have already been published on the subject [180–189]. Extensive reviewing of the field would be inappropriate in this context, our purpose being only that to compare the redox behaviour of MCC with those of nanometre-sized alkanethiolate monolayer-protected gold clusters (MPC). We shall only outline some of their problematic and their relevant features for sake of comparison.

The first breakthrough in the field of narrow-dispersed colloidal particles has been the report by Schmid in 1981 of $Au_{55}(PPh_3)_{12}Cl_6$ [190]. The major impulse was, however, given by the discovery that alkanethiols enable the synthesis of MPC featuring diameters in the 1–5 nm range [191], which can be dissolved and fractionally separated by precipitation up to obtain almost mono-dispersed materials. Since only crystals of micrometer size have been so far obtained, their characterisation was achieved on combining several experimental techniques (mainly high-resolution electron microscopy, transmission electron microscopy, electron diffraction, X-ray powder diffraction and laser desorption mass spectrometry) with theoretical modelling and simulation. Cubic-close-packed lattices are by far predominant and the optimal structures are predicted to be based on truncated octahedra of increasing frequency, while the likely identity is inferred by mass spectrometry [181].

From a formal point of view, there is a remarkable similarity between the electroanalytical responses of MCC and MPC. Thus, the cyclic and differential pulse voltammetric profiles of C_6S–$Au_{140-147}$, an ensemble of almost mono-dispersed hexanethiol-MPC (differently formulated on dependence of preparation/fractionation procedures and authors) in solution has been initially reported to feature 10 redox changes [156,157]. Their number increases up to 13 on lowering the temperature [158] and up to 15 on improving mono-dispersity [159]. Residual dispersity in core size is thought to contribute to peak broadening and background. Within the -0.2 and -1.9 V window, which is the one of interest for anionic MCC with electron-sink properties, the CV and DPV profiles of miscellaneous C_xS–$Au_{140-147}$ ($x = 6$–12) are strictly comparable with those shown by high-nuclearity MCC such as $[Ni_{32}C_6(CO)_{36}]^{6-}$ and $[Ni_{38}Pt_6(CO)_{48}]^{6-}$. Furthermore, the pattern of CV and DPV of C_6S–Au_{38} [156] is very similar to that of low-nuclearity MCC such as for instance $[HRh_{14}(CO)_{25}]^{3-}$ and $[Pt_{19}(CO)_{22}]^{4-}$. Compare the z-plots of Fig. 13 with those of Figs. 8 and 9.

According to Eq. (3), capacitance should rise upon increasing the radius r of the metal particle and decrease by increasing the thickness d of the monolayer of ligands. MPC give the opportunity to keep r practically constant and to vary the thickness d of the protecting monolayer by varying the chain length of thiols. Measurements performed on C_xS–Au_{145} species, which have a constant radius of the metal core of 0.8 nm and x varying from 4 to 16, are in keeping with Eq. (3) by disclosing a capacitance that reduces from 0.59 to 0.39 aF [157]. MCC feature almost constant thickness of the shell of carbonyl groups and a variable radius of the metallic core. They are, therefore, complementary to MPC. As anticipated in Section 4.5, the capacitance of MCC so far subjected to electroanalytical experiments increases from
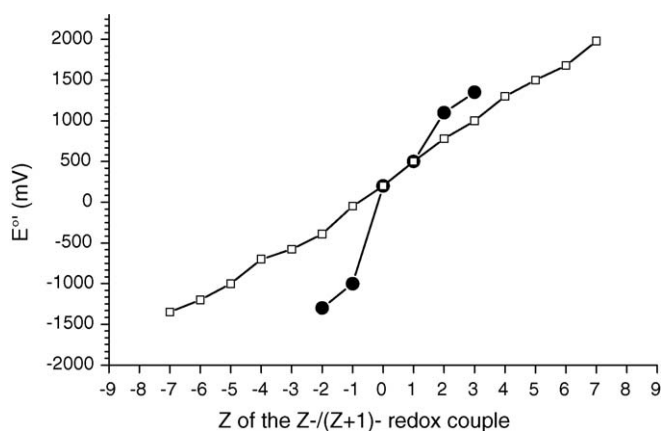

Fig. 13. *z*-Plot vs. $E^{\circ\prime}$ of C6S-Au$_{147}$ (□) and C6S–Au$_{38}$ (●) MPC, respectively showing a linear and staircase trends.

0.21 to 0.57 aF as the nuclearity increases. Rewardingly, both results are in keeping with Eq. (3).

Finally, it is important to take note of the remarkable correspondence between the solution electrochemical response of MPC ensembles and the tip-based tunnelling spectroscopy of an individual MPC physisorbed on a gold-on-mica support. The STM tip experiment on the latter displays a reversible coulombic staircase with six charging steps constantly separated by ca. 0.34 V [156]. A Coulombic blockade has been ascertained also in $Au_{55}(PPh_3)_{12}Cl_6$ [171].

6. Assembling metal carbonyl clusters: new functional materials of potential interest for nanoscience and nanotechnologies

The condensation of MCC moieties, of which some example has been anticipated at the end of Section 4.4, has been or could in principle be obtained in several ways. A few documented procedures enabling oligomerisation of MCC are:

1. Oxidation of an anionic MCC with formation of new direct homonuclear M–M bonds (e.g. oxidation of $[Pt_6(CO)_{12}]^{2-}$ to $[Pt_{12}(CO)_{24}]^{2-}$, $[Pt_{18}(CO)_{36}]^{2-}$, etc. [192]).
2. Condensation of anionic MCC with $[M']^{z+}$ ($z = 1$–3) cations, via complete elimination of counterions and, in case, some carbon monoxide, by formation of heteronuclear M–M′–M bonds (e.g. $\{Ag[Rh_6C(CO)_{15}]_2\}^{3-}$ [177], $\{Hg[Os_{10}C(CO)_{24}]_2\}^{2-}$ [172], $[M_2Ru_{12}C_2(CO)_{30}]^{2-}$ (M = Pd, Ag) [193,194], $[Pd_3Os_{18}C_2(CO)_{42}]^{2-}$ [195] and $[Ni_{12}(\mu_6\text{-}In)(\eta^2\text{-}\mu_6\text{-}In_2Br_4OH)(CO)_{22}]^{4-}$ [196]).
3. Condensation of anionic MCC with $M'X_n$ salts of Groups 11–13, with incomplete elimination of X counterions and formation of heteronuclear M–M′X$_{n-1}$–M or M–M′$_nX_m$–M metallic interactions (e.g. $[H_2Ru_{12}Cu_6Cl_2(CO)_{34}]^{2-}$ [174], $[H_4Ru_{20}Cu_6Cl_2(CO)_{48}]^{4-}$ [175], and $[Ag_3Ru_{10}C_2(CO)_{28}Cl]^{2-}$ [176]).
4. Condensation of anionic MCC with $M'X_n$ salts of Groups 11–13, with limited or without elimination of X counterions and formation of heteronuclear M–M′ interactions and M'–X → M′ bridges (e.g. $\{Cd_2Cl_3[Ni_6(CO)_{12}]_2\}^{3-}$ [173]).
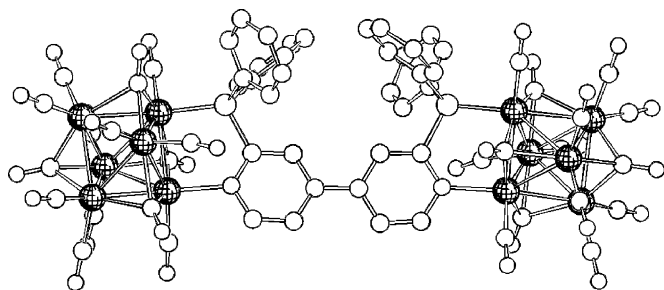
Fig. 14. The structure of $\{[Rh_6(CO)_{14}]_2(dpbp)\}$ (dpbp = 2,2'-bis(diphenyl-phosphino)-4,4'-bipyridine) [198].

5. Condensation of anionic, neutral or cationic MCC with a neutral or anionic bridging ligand such as (but not limited to) diamines, diphosphines or dithiolates, via formation of M–L–L–M bonds (e.g. $\{H_2N–(CH_2)_4–NH_2\}$-$[Rh_5(CO)_{14}]_2\}^{2-}$ [197], $\{[Rh_6(CO)_{14}]_2(dpbp)\}$ (see Fig. 14) and $\{Ru_6C(CO)_{15}(dpbp)_3]Ir_4(CO)_8\}$ (dpbp = 2,2'-bis(diphenylphosphino)-4,4'-bipyridine) [198].

Procedures 1–3 afford new MCC of greater size, which imply metal architectures essentially or uniquely sustained by M–M or M'–M metallic bonds. Procedures 4 and 5 lead to species in which MCC moieties are not joined by a direct M–M or M–M' bond and may feature conducting or insulating bridges. Expected properties of some of the above aggregates, once assembled by using redox-active MCC, are enhanced electron-sink behaviour and mixed-valence clusters, formally related to $Rh_6(CO)_5(dppm)_2(CNCH_2Ph)(C_{60})_2$ [199]. Notice that bis-fullerenes exhibit a weak through-space electronic communication and undergo 2-electron reductions with ΔEs of ca. 0.45 V, practically coincident with those of C_{60} [200–202]. On the contrary, the MCC bridge of $Rh_6(CO)_5(dppm)_2(CNCH_2Ph)(C_{60})_2$ tremendously enhances communication between the two C_{60} moieties. The species undergoes sequential one-electron reductions, twice as much with respect to C_{60} and displaying ΔEs between consecutive redox couples decreased at 0.19–0.29 V [199]. Therefore, the above purported bis-MCC species, as a function of the conducting behaviour of the bridge, would enable investigation of intramolecular electron-transfer processes between the two MCC units and beyond.

At least in principle, all above procedures 1–5 could also enable self-assembly of a variety of 1D molecular wires. Both physicists and chemists have been and are still fascinated by 1D or pseudo-1D materials. As this topic ranges over organic, inorganic and organometallic chemistry, an impressive vastness of literature is already available. Therefore, we will limit to suggest some dedicated readings [203,204], and we will introduce the subject as briefly as possible by citing only some historical example, e.g. the 1D stacked square-planar d^8 coordination compounds attaining short M–M contacts along the stack upon doping (e.g. $K_2[Pt(CN)_4]X_{0.3}\cdot 3H_2O$ [205]) or in donor–acceptor relation with almost parallel stacks of organic molecules (e.g. $[TTF][M(dmit)_2]$ (M = Ni, Pd; dmit = 4,5-dimercapto-1,3-dithiole-2-thione) [206], α-[EDT-

TTF][Ni(dmit)_2] (EDT-TTF = ethylenedithiotetrathia fulvalene [207]), the mixed-valence stacks of donor and acceptor organic molecules such as [TTF][TCNQ] (TTF = tetrathiafulvalene, TCNQ = 7,7',8,8'-tetracyanoquinodimethane) [208]) or [TMTSF]_2[ClO_4] (TMTSF = tetramethyltetraselenafulvalene) [209], as well as conducting organic polymers such as poly-acetylene, pyrroles and tiophenes [210,211]. The discovery of their conducting or superconducting behaviour, combined with physical theories anticipating high-Tc 1D superconductors [212,213], continuously stirred up the field.

One recent example of molecular metal wire provided by coordination chemistry is the mixed-valence $\{[Rh(CH_3CN)_4][BF_4]_{1.5}\}_\infty$ derivative obtained by electro-crystallisation of $[Rh_2(CH_3CN)_{10}][BF_4]_4$ at a Pt electrode [214,215]. However, in spite of the presence of an infinite sequence of alternate Rh–Rh contacts of 2.84 and 2.93 Å and mixed-valence Rh centres, the above molecular metal wire displays charge transport behaviour of a semiconductor [214].

6.1. 1D and 2D molecular arrays by self-assembly of metal carbonyl clusters

Molecular metal wires involving metals in positive oxidation states and carbon monoxide as ligand have been known for a long time. For instance, several carbonyl halides such as $Ir(CO)X_3$ (X = Cl, Br) [205], $Rh(CO)_2(acac)$ [216] or $Pt(CO)_2Cl_2$ [217] crystallise as infinite stacks with M–M separations 10–20% longer than distance in the bulk metal. Some of them shows metal conductivity upon doping [205]. A more recent example involving M–M bonds supported by ligands is $\{[Rh_2(CF_3COO)_4][Rh_2(CF_3COO)_2(CO)_4]_2\}_\infty$ [218,219].

Molecular metal wires assembled by metals in zero or negative oxidation states and carbonyl groups as only ligands are more rare. To our knowledge the first structurally characterised example has been $[CuCo(CO)_4]_\infty$ [220]. This compound derives by self-assembly of $[Co(CO)_4]^-$ with Cu^+ ions, which can give rise either to a cyclic $[Cu_4\{Co(CO)_4\}_4]$ tetramer or an infinite 1D $[CuCo(CO)_4]_\infty$ isomer displaying a zigzag chain of metal atoms, as a function of the crystallisation procedure. A linear $[Ru(CO)_4]_\infty$ infinite chain of metal atoms has recently been determined by X-ray powder diffraction for the red modification of $Ru_3(CO)_{12}$ [221]. This has been known for a long time but was never characterised before, owing to difficulties in obtaining suitable crystals [222]. In the context of the present section, however, the most pertinent example is the recently reported $\{[AgRu_6C(CO)_{16}]^-\}_\infty$ infinite superwire [194]. It has been quantitatively assembled by reaction of equimolar amounts of $[Ru_6C(CO)_{16}]^{2-}$ clusters and Ag^+ ions and, therefore, can be taken as an example of condensation procedure 2, which self-stretches to infinity. The formation of infinite chains of ruthenium clusters and silver atoms in the crystalline state is suggested to be aided by the comparable size of $[Ru_6C(CO)_{16}]^{2-}$ cluster and $[N(PPh_3)_2]^+$ or $[PPh_4]^+$ counterions. Both salts are soluble in acetone, probably owing to breakdown into oligomers, and can be recovered quantitatively upon precipitation [194]. This ready dis- and re-assembling is an important feature for possible applications outlined later.

Incipient self-assembly of MCC units is displayed by the $[NMe_4]_2[Ni_6(CO)_{12}]$ salt [223,224]. The $[Ni_6(CO)_{12}]^{2-}$ cluster ions are pillared in ordered columns, so that there is an infinite sequence of staggered and eclipsed $Ni_3(CO)_6$ moieties alternately separated by a ca. 2.5 bonding and 4.5 Å non-bonding contacts [224]. A further hint that incompletely carbonyl-shielded $[M_{3n}(CO)_{6n}]^{2-}$ (M = Ni, Pt) and $[Pt_{26}(CO)_{32}]^{2-}$ clusters can aggregate to oligomers built by up to 20–30 units came from ^{252}Cf plasma desorption mass spectrometry [225].

In the search of such materials, we have adopted a modification of procedure 1. The change consists in the use of dications which behave as mild oxidising agents and cannot establish covalent bonds with MCC. Possible examples of such cations are the redox-active 1,1′-disubstituted-4,4′-bipyridilium dications (viologens) [226], which exhibit formal redox potentials comparable to those of MCC and tunable as a function of 1,1′-substituents. Thus, metathesis of preformed $[Pt_{3n}(CO)_{6n}]^{2-}$ (n = 3–5) salts with 1,1′-diethyl-4,4′ bipyridilium dication (Et–V^{2+}) affords the mixed $[Et–V^{2+}][Et–V^{\bullet+}]_2[Pt_{15}(CO)_{30}]_2$ salt containing both the starting Et–V^{2+}, as well as the Et–$V^{\bullet+}$ radical mono-cation [227]. Two views of the $[Et–V^{2+}][Et–V^{\bullet+}]_2[Pt_{15}(CO)_{30}]_2$ packing, one perpendicular to the other, are shown in Fig. 15. The two different diethyl viologen cations are clearly distinguishable by their frequency in the lattice and the fact that Et–V^{2+} is twisted, while Et–$V^{\bullet+}$ is substantially flat. The most interesting feature of the structure is that $[Pt_{15}(CO)_{30}]^{2-}$ dianionic moieties, even though maintain their molecular identities, are assembled in infinite columns. Within each molecular ion the $Pt_3(CO)_6$ interlayer distances are slightly less than 3.1 Å, while the intermolecular distance (ca. 3.9 Å) is shorter than in $[NMe_4]_2[Ni_6(CO)_{12}]$ (4.5 Å) and close to twice the likely van der Waals radius of platinum(0). According to Hoffmann [228], an extended pillar of $[Pt_3(CO)_6]$ moieties would be characterised by development of an energy band along the pillar. Partially filled bands can result in structural Peierls distortions (dimer for one-half-, trimer for one-third-, tetramer for one-quarter-filled, etc. metallic band) [229]. From a solid-state point of view, the ordered alternance along the columns of four short 3.1 and one long 3.5 Å contacts could signal the occurrence of Peierls distortions in 1D stack of $[Pt_3(CO)_6]^{0.4-}$ units. Implicit in this interpretation is that progressive electron depletion of the band should result in progressively higher oligomers and, perhaps, conducting molecular wires. The above considerations suggested further tuning of the formal redox potentials of the viologen dication. Substitution of both 1,1′ ethyl groups with $-CH_2-C(=O)-OEt$ and $-CH_2-C\equiv N$ moieties significantly increases the oxidising power of the viologen dication [226]. By repeating the metathesis of sodium salts of preformed $[Pt_{3n}(CO)_{6n}]^{2-}$ (n = 3–5) dianions with the above dications, crystals of two new salts of very similar structural motif, showing small but significant differences, have been isolated [230].

The packing of $Pt_3(CO)_6$ units in the $[EtO-C(=O)-CH_2-V]^{x+}$ salt is shown in Fig. 16. Infinite pillars of equidistant (3.2 Å) and perfectly eclipsed $Pt_3(CO)_6$ units are arranged in squeezed hexagons. $[EtO-C(=O)-CH_2-V]^{x+}$ cations and solvent molecules probably fill the hexagonal channels. Unfor-
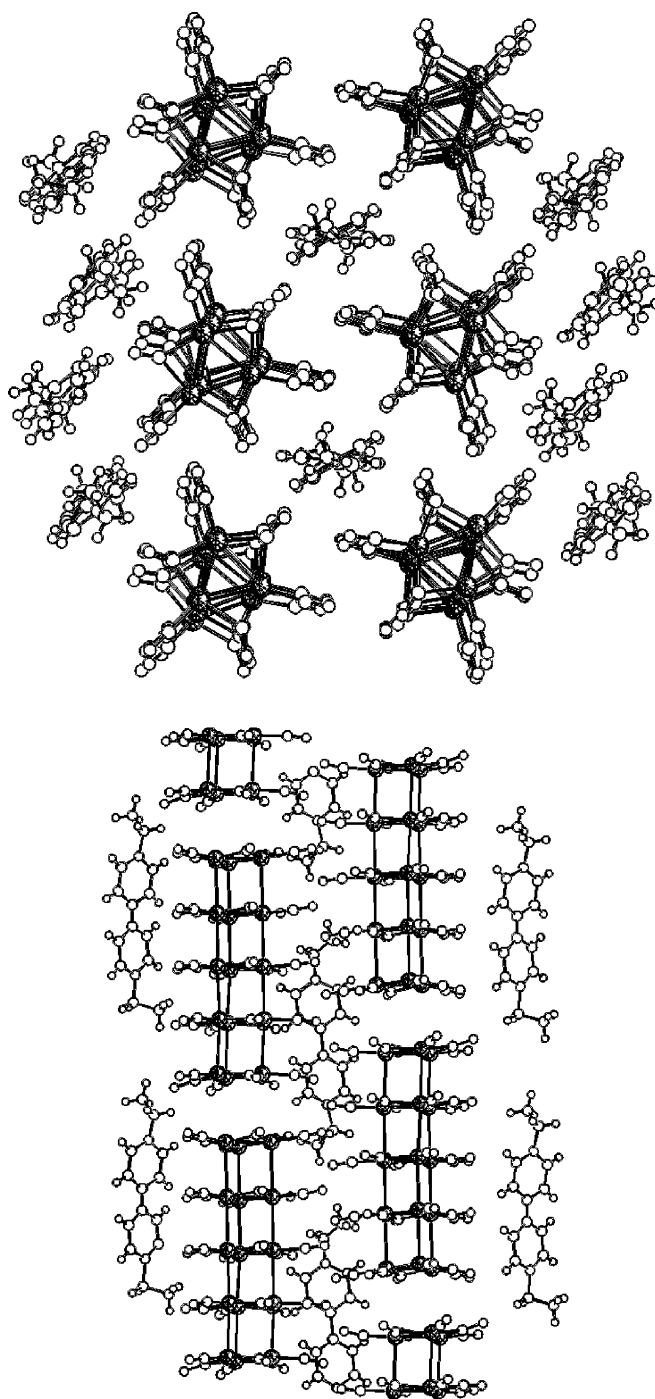
Fig. 15. Two views of the crystal packing of $[Et–V^{2+}][Et–V^{\bullet+}]_2[Pt_{15}(CO)_{30}]_2$.

tunately, the number and nature of both cations and solvent molecules could not be unravelled, likely due to their small contribution to diffraction and lack of sufficiently good X-ray diffraction data even at low temperature (100 K). Several different unit cells with a varying c axis and comprising seven or more $Pt_3(CO)_6$ units could be adopted. All gave similar disappointing results. Therefore, the average charge of each $Pt_3(CO)_6$ unit is yet undetermined. Similar problems hampered full elucidation of the structure of the related $[N\equiv C-CH_2-V]^{x+}$ salt.

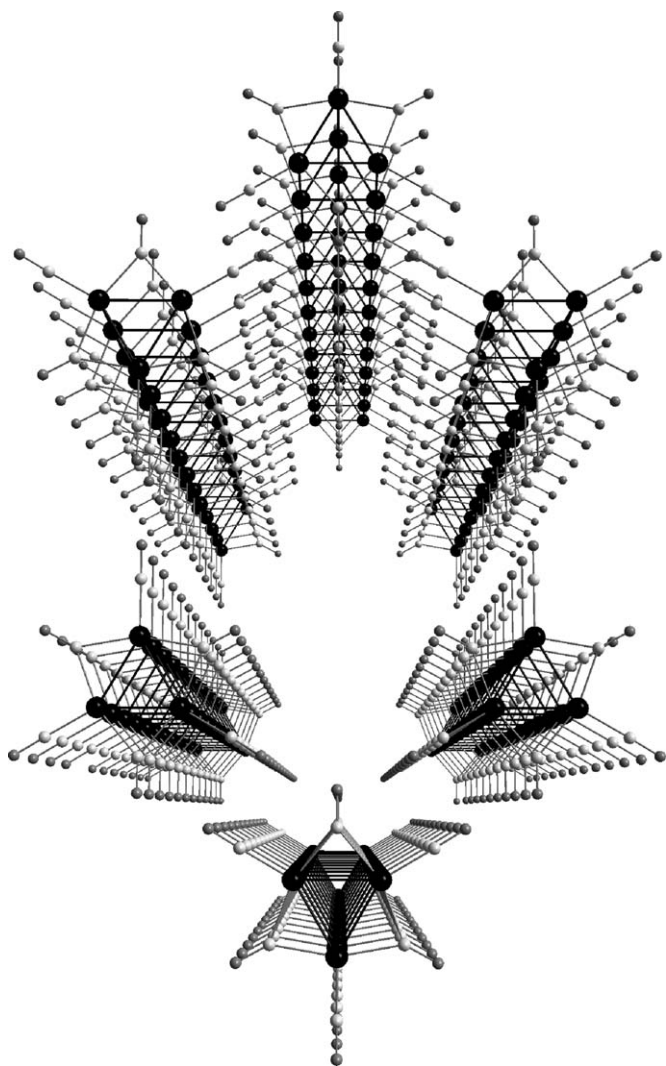Fig. 16. The $[Pt_3(CO)_6]_\infty^{n-}$ columns of the $[EtO-C(=O)-CH_2-V]^{x+}$ salt.

As an example of procedure 4, the reaction of $[Pt_9(CO)_{18}]^{2-}$ with $CdCl_2$ affords a molecular $[Pt_9(CO)_{18}(\mu_3-CdCl_2)_2]^{2-}$ adduct, which self-assembles into a molecular $\{Cd_2Cl_4[Pt_9(CO)_{18}]^{2-}\}_\infty$ 1D superwire via chloride bridges upon crystallisation [173]. Its crystals are soluble in several organic solvents owing to ready and complete depolymerisation.

Somehow related to procedure 5 is the remarkable condensation via isocarbonyl groups of an anionic MCC, the previously unknown $[Co_4(CO)_{11}]^{2-}$, with Yb(II) and Eu(II) cations which gives rise to 1D and 2D array, as a function of rare-earth coordinated solvent [231]. Coordination of THF to Eu(II) favours isocarbonyl linkages of the kind η^2,μ_4 and leads to the 1D zigzag chain structure of $\{(THF)_5Eu[Co_4(CO)_{11}]\}_\infty$. In contrast, the tri-solvated $\{(Et_2O)_3Ln[Co_4(CO)_{11}]\}_\infty$ (Ln = Yb, Eu) and $\{(Et_2O)_2(THF)Yb[Co_4(CO)_{11}]\}_\infty$ compounds display puckered 2D arrays built by four- and eight-membered rings via η^2,μ_4 and η^2,μ_3 isocarbonyl networking. To our knowledge, these represent the first examples of 2D arrays built by MCC, whereas 2D and 3D polymers by assembly of halide and pnicogenide clusters are already common and actively investigated as nanoporous materials [232].

6.2. Charge- or electron-transfer materials based on salts of redox-active anionic clusters and redox-active countercations

A few viologen salts of polynuclear compounds of metals in high oxidation state have already been reported [226]. To our knowledge, however, none of the investigated polynuclear compounds featured redox behaviour. Electro-active organic cations with formal redox potentials tuned with those of redox-active MCC, such as those reported in Table 3, could enable the preparation of new charge- or electron-transfer salt-based materials [233]. So far the only reported example is $[Et-V^{\bullet+}]_5[Ag_{13}Fe_8(CO)_{32}]$ [132]. This salt has been obtained by reaction of $[Ag_5Fe_4(CO)_{16}]^{3-}$ with $[Et-V^{2+}]$ diiodide. Owing to low solubility in THF $[Et-V^{\bullet+}]_5[Ag_{13}Fe_8(CO)_{32}]$ separates out as a dark-green powder. The salt is soluble in DMF with green colour and has been crystallised by layering isopropyl alcohol. Both solution and crystalline solid have been spectroscopically investigated. Notably, the solution showed IR carbonyl absorptions identical to those of the odd-electron $[Ag_{13}Fe_8(CO)_{32}]^{4\bullet-}$ tetraanion but only the EPR signal of Et–V$^{\bullet+}$ radical cation. Analogously, the crystals showed a strong EPR signal due to the cation, while a broad doublet typical of $[Ag_{13}Fe_8(CO)_{32}]^{4\bullet-}$ in the solid state became visible only at very high gain. Therefore, in view of the presence in the crystal structure of five cations per each anion, the latter has been formulated as the even-electron $[Ag_{13}Fe_8(CO)_{32}]^{5-}$. A comparison of its molecular parameters with those of the previously characterised $[Ag_{13}Fe_8(CO)_{32}]^{3-}$ [234] and $[Ag_{13}Fe_8(CO)_{32}]^{4\bullet-}$ [235] lends support to the above conclusion, by showing significant shortening of Ag–Ag and elongation of Ag–Fe bonds, as the negative charge of the anion increases. By integration of the EPR signals the $[Ag_{13}Fe_8(CO)_{32}]^{5-}/[Ag_{13}Fe_8(CO)_{32}]^{4\bullet-}$ ratio at least amounts to 30 or more. The above findings are in keeping with occurrence of charge-transfer between anion and cation in solution and electron-transfer in the solid state. However, it should be mentioned that tetrasubstituted ammonium or phosphonium salts of even-electron $[Ag_{13}Fe_8(CO)_{32}]^{3-}$ and $[Pt_3Fe_3(CO)_{15}]^{2-}$ often were found to contain trace-amount impurities of their odd-electron congeners. The identical structure and dimensions of the $[Ag_{13}Fe_8(CO)_{32}]^{4\bullet-}-[Ag_{13}Fe_8(CO)_{32}]^{5-}$ and $[Pt_3Fe_3(CO)_{15}]^{\bullet-}-[Pt_3Fe_3(CO)_{15}]^{2-}$ pairs of molecular cluster ions favour the association also of the second ion of each pair in the crystal lattice, every time impurities of the second ion are present during crystallisation. That would argue against the conclusion that the presence of $[Ag_{13}Fe_8(CO)_{32}]^{4\bullet-}$ in the crystals of $[Et-V^{\bullet+}]_5[Ag_{13}Fe_8(CO)_{32}]$ is due to an electron-transfer process in the solid state. In any case, observation of a coupling constant of the unpaired electron of $[Ag_{13}Fe_8(CO)_{32}]^{4\bullet-}$ with the unique interstitial silver atom, identical to that observed in the presence of tetrasubstituted ammonium or phosphonium cations, points out that all conceivable intermolecular electron-transfer processes (anion-to-anion as well as anion-to-cation) are slow in comparison to EPR time-scale.

The structure of $[Et-V^{\bullet+}]_5[Ag_{13}Fe_8(CO)_{32}]$ is shown in Fig. 17. A potentially interesting feature of the packing is the

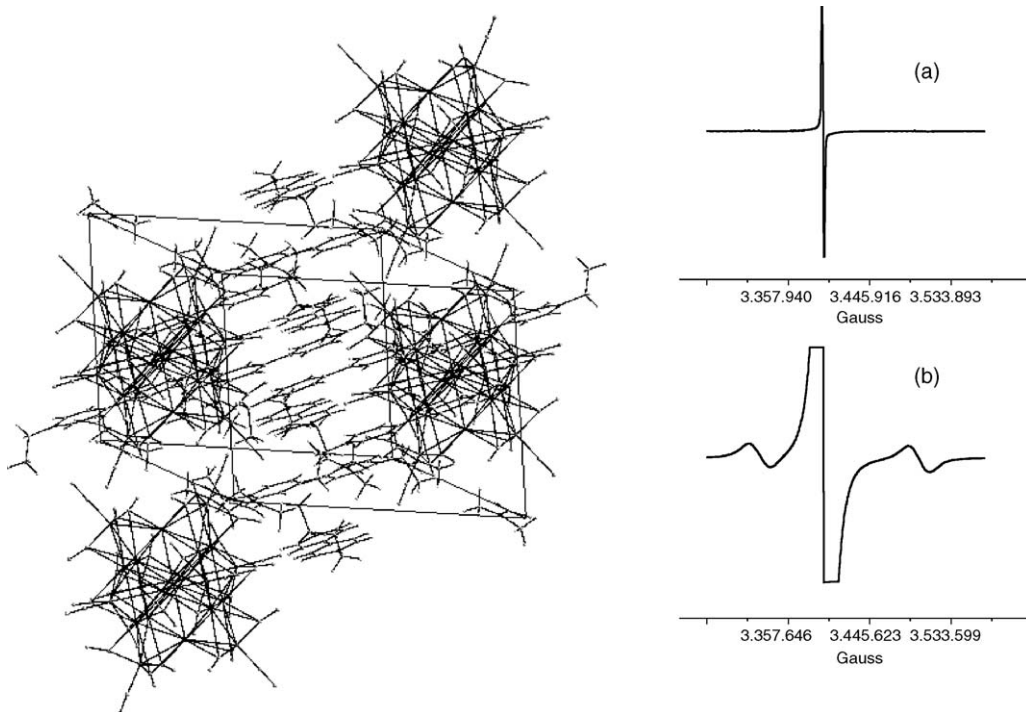Fig. 17. View along the *a* axis of the unit cell of [Et–V$^{\bullet+}$]$_5$[Ag$_{13}$Fe$_8$(CO)$_{32}$] and EPR spectrum of the crystals at low (a) and at high (b) gain.

presence of layers of stacked Et–V$^{\bullet+}$ cations alternated with layers of [Ag$_{13}$Fe$_8$(CO)$_{32}$]$^{5-}$ anions. The stacking motives of Et–V$^{\bullet+}$ mono-cations in [Et–V$^{\bullet+}$]$_5$[Ag$_{13}$Fe$_8$(CO)$_{32}$] is shown in Fig. 18. Pentameric aggregates displaying inter-planar distances of ca. 3.25 Å and slightly longer inter-aggregate distances of 3.6 Å are clearly distinguishable.

Stacks of Me–V$^{\bullet+}$ (Me–V$^{\bullet+}$ = 1,1′-dimethyl-4,4′-bipyridilium cation) with an angle of 37° relative to one another and a constant inter-planar separation of 3.29 Å were found in the almost black crystals of its PF$_6^-$ salt. Notably, within the stack there are alternated Me–V$^{\bullet+}$ moieties revealing distinct interannular C–C bond distances of 1.44 and 1.40 Å. These have been assumed to indicate a Me–V$^{\bullet+}$ Me–V$^{\bullet+}$ ↔ Me–V^{2+} Me–V^0 resonance deriving from a charge-transfer or self-complexation process [236].

The interannular distances of Et–V$^{\bullet+}$ cations of [Et–V$^{\bullet+}$]$_5$ [Ag$_{13}$Fe$_8$(CO)$_{32}$] are strictly comparable to the above. It is however worth remarking that attempts to assemble new charge- or electron-transfer salt-based materials ended beyond in giving also 1D stacks of organic radical cations with interplanar separation closer than graphite. The pillaring of Et–V$^{\bullet+}$ cations is probably induced by the stoichiometry of the salt, which requires five mono-cations per each anionic moiety. EHMO calculations suggest a weak σ-interaction along the stack between the π-MOs of Et–V$^{\bullet+}$ radical cations, which would give rise either to a half-filled set of MOs in the pentameric aggregate of [Et–V$^{\bullet+}$]$_5$[Ag$_{13}$Fe$_8$(CO)$_{32}$]. Preliminary measurements indicate that substitution of tetrasubstituted ammonium cations with viologen di- and mono-cations decreases the solid-state resistivity of these materials of orders of magnitude.
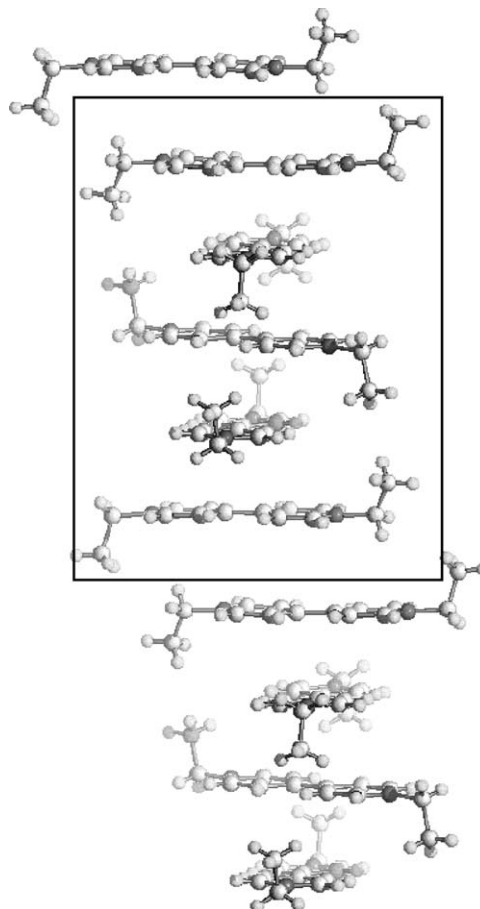

Fig. 18. The stack of Et–V$^{\bullet+}$ radical cations found in the [Et–V$^{\bullet+}$]$_5$[Ag$_{13}$Fe$_8$ (CO)$_{32}$] crystal structures. The rectangle points out the repeating unit in the stack.

7. Perspectives of nanolithography with monolayers of metal carbonyl clusters

We will now progressively venture in an increasingly speculative territory with the wish to envision some future development for MCC chemistry. Molecular capacitors such as MCC appear to deserve some consideration in molecular electronics as building units to assemble re-writable memories, as well as applications in destructive nanolithography. Unquestionable disadvantages are represented by their air sensitivity and limited thermal stability. Their handling and study has to be done under strictly anaerobic conditions. However, some advantages arising from their nature and properties can be envisaged. Even their limited stability may turn out to be an advantage in some applications. Applications as re-writable memories or in destructive nanolithography requires in primis assembly of MCC into monolayers or Langmuir–Blodgett films. Surfaces nano-structured with clusters so far reported have been obtained via weak van der Waals interactions between cluster molecules and the substrate (e.g. $Rh_4(CO)_{12}$ and $[Pt_{12}(CO)_{24}]^{2-}$ on highly oriented pyrolytic graphite [237], $Au_{55}(PPh_3)_{12}Cl_6$ and $C_xS–Au_{140}$ MPC on a variety of supports [181,238–243]), $Fe_4Cp_4S_4$ and $Pt_5(CO)_6(PPh_3)_4$ on stearic acid [244]. With the great majority of MCC of Table 2 one could additionally profit of electrostatic interactions. It appears conceivable to think that both inorganic surfaces and organic polymers functionalised with cationic nitrogen moieties could be nano-structured by simple dipping into solutions of anionic MCC owing to electrostatic interactions.

Furthermore, molecular wires such as the previously described $\{[N\equiv C–CH_2–V]_x[Pt_{3y}(CO)_{6y}]\}_\infty$, $\{[AgRu_6C(CO)_{16}]^-\}_\infty$, $\{Cd_2Cl_4[Pt_9(CO)_{18}]^{2-}\}_\infty$ or 2D arrays such as those exemplified by the tri-solvated $\{(Et_2O)_3Ln[Co_4(CO)_{11}]\}_\infty$ (Ln = Yb, Eu) and $\{(Et_2O)_2(THF)Yb[Co_4(CO)_{11}]\}_\infty$ compounds can perhaps be assembled and linked to inorganic or polymer surfaces, for instance, by partial substitution of pending chlorides or coordinated solvents with donor functionalities of the surface. Electrostatic interactions or coordinative linkages may provide procedures additional to the reported techniques for self-assembling ordered monolayer arrays of nanoparticles on solid surfaces [243]. Materials such as those envisioned above may be amenable to studies as re-writable memories or find applications in destructive nanolithography.

7.1. Envisioning molecular lithography and information storage

Molecular electronics [245] consist in the direct measurement of the electronic behaviour of a single molecule. The electronic properties of molecules have been investigated for years in the gas or solid phase and in solution with photons. Electrical circuits using photons as control elements cannot be reduced to nanometer-scale dimensions. In contrast, the tip of a scanning tunnelling microscope (STM) or a conducting tip of an atomic force microscope (AFM) can interrogate single molecules and measure their current versus voltage characteristics. Indeed, Pt/Ir
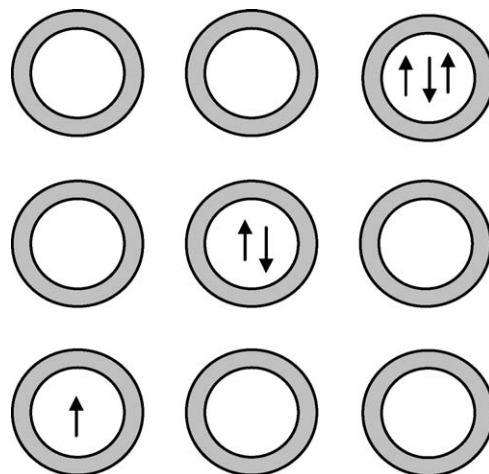

Fig. 19. Cartoon of an ordered monolayer of differently charged individual MCC capacitors in consequence of their electron-sink properties and the insulating behaviour of their CO shell.

or W tips can be made so sharp to reach a precision of 0.1 nm on *x* and *y* and 0.01 nm on the vertical *z*-axis [186].

Imagine a surface covered by an ordered monolayer array of redox-active MCC of nanometer size, such as the one depicted in the cartoon of Fig. 19. A STM or AFM tip can be moved across the surface to reach a given nanocapacitor and drop one electron into it at a specific voltage and reversibly store a bit of information. This "on" molecular nanocapacitor will exhibit a different voltage response from other surrounding "off" nanocapacitors. The result would be a readable, modifiable, erasable and re-writable surface. In such a way, molecular lithography and data storage could be pursued.

Furthermore, more than one electron can be dropped in a single molecular nanocapacitor. Stepwise increase of voltage should allow charging with two, three or more electrons. Therefore, not only binary but even more complex logics can be implemented [246]. The inherently low speed with which the STM or AFM tips can be moved across the surface to reach a given location can be compensated to a certain extent by using devices such as the "Millipede" developed at IBM. This consists of an array of 32×32 of closely spaced microfabricated AFM cantilevers, which could be independently operated as reading or writing devices [247,248].

7.2. Envisioning destructive nanolithography

It has been demonstrated that nanoscale patterning of Langmuir–Blodgett films of gold nanoparticles by electron-beam lithography is viable [249]. A gold graffiti has been produced onto a surface nano-structured with gold MPC by selectively burning rows of nanoparticles with an electron beam. Washing away the yet soluble unexposed nanoparticles with solvent left painted gold nanograffitis 20–50 nm wide on the support. A related patterning should be possible also onto monolayers or Langmuir–Blodgett films of MCC anchored by electrostatic or coordinative interactions onto a surface. Indeed, most MCC will be burned by exposure to a sufficiently intense elec-

tron beam. Several years ago Analytical Electron Microscopy experiments on $[HNi_{38}Pt_6(CO)_{48}]^{5-}$ salts deposited on a grid showed that upon varying the intensity of the electron beam the original molecular cluster underwent a series of transformations up to formation of spots of the Ni_3Pt superalloy. Related decompositions to metals or alloys were also featured by several other MCC of different metal compositions [250–252]. For such destructive applications a nanometric size of MCC is probably not necessary and that would open the field to a variety of homo- and heterometallic MCC with compositions including most elements of Periodic Table. Furthermore, nano-patterning of surface with metal wires or dots could eventually take advantage from the possibility to deposit and link to surfaces molecular wires and 2D networks by self-assembly of MCC.

Most MCC are also unstable to UV and laser radiation, and are thermally decomposed to metal very often below a temperature of 200 °C. These can turn out to be alternative opportunities for the preparation of nanometer-sized architectures on surfaces.

8. Conclusions

In concluding this survey of the possible role that metal carbonyl clusters could play in nanoscience and nanotechnologies, based on their documented but, deliberately, also on perhaps visionary chemistry of MCC, it would be completely improper to omit any mention of their most promising application in nanotechnologies: MCC as precursors of nanometric metal particles for catalysis. MCC have been synthesized by diffusion of suitable starting coordination compounds through the small windows and channels interconnecting the larger cages of some microporous material and self-assembled and trapped inside the above cavities, the so called "ship-in-a-bottle" technique. The cages and channels have also a function of template [253]. Larger and preformed MCC have been directly introduced in the channels of mesoporous materials by diffusion and adsorptions. Subsequent mild thermal treatments produce metal nanoparticles or nanowires trapped within the cages or anchored along the channels. In the case of preformed MCC the metal particles dispersed inside the channels substantially maintain the size and composition of the parent MCC [176]. All above nanomaterials display enhanced activity, selectivity and stability with respect to their corresponding conventionally prepared catalysts. However, since several authoritative reviews, written by the most prominent contributors to the field, are already available in literature [254–257], extensive reviewing by us would have been inappropriate.

The above achievements, the most recent outcome of MCC chemistry described in the initial sections and the developments outlined in the last sections would have appeared visionary to several readers in the recent past. It seems justified to conclude that MCC chemistry continues to spring exciting new results and fuels continuous interest. Structurally and compositionally well-defined MCC of nanometric size had yet a poor impact in nanotechnologies, other than heterogeneous catalysis, when compared with molecularly less-defined quasi monodispersed ligand-stabilised metal nanoparticles. This could be due, beyond other considerations, to a widespread opinion that

their synthesis and purification is troublesome. It is up to cluster chemists to provide more tailored and easy-reproducible separations and syntheses. However, in order to understand and exploit in nanoscience and nanotechnologies the chemical properties of MCC which are being uncovered, there is undoubtedly an absolute need to combine and concert future efforts of chemists, physicists and material scientists.

Acknowledgement

References

[1] U. Simon, in: P. Braunstein, L.A. Oro, P.R. Raithby (Eds.), Metal Clusters in Chemistry, vol. 3, Wiley–VCH, Weinheim, 1999, p. 1342.
[2] G. Schmid, Y.-P. Liu, M. Schumann, T. Raschke, C. Radehaus, Nano Lett. 1 (2001) 405.
[3] S. Hoeppener, L. Chi, H. Fuchs, Nano Lett. 2 (2002) 459.
[4] M.H.V. Werts, M. Lambert, J.-P. Bourgoin, M. Brust, Nano Lett. 2 (2002) 43.
[5] A.C. Templeton, W.P. Wuelfing, R.W. Murray, Acc. Chem. Res. 33 (2000) 27.
[6] L.F. Chi, M. Hartig, T. Drechsler, T. Schwaack, C. Seidel, H. Fuchs, G. Schmid, Appl. Phys. Lett. 66 (1998) S187.
[7] D.F. Shriver, H.D. Kaesz, R.D. Adams (Eds.), The Chemistry of Metal Cluster Complexes, VCH, New York, 1990.
[8] D.M.P. Mingos, D.J. Wales, Introduction to Cluster Chemistry, Prentice Hall, Englewood Cliffs, 1990.
[9] J.P. Fackler (Ed.), Metal–Metal Bonds and Clusters in Chemistry and Catalysis, Plenum, New York, 1992.
[10] B.C. Gates, Catalytic Chemistry, Wiley, New York, 1992.
[11] G. Gonzalez-Moraga, Cluster Chemistry, Springer Verlag, Berlin, 1993.
[12] C.E. Housecroft, Metal–Metal Bonded Carbonyl Dimers and Clusters, Oxford Science Publisher, Oxford, 1994.
[13] G. Schmid (Ed.), Clusters and Colloids: From Theory to Applications, VCH, Weinheim, 1994.
[14] L.J. De Jongh (Ed.), Physics and Chemistry of Metal Cluster Compounds, Kluwer, Dordrecht, 1994.
[15] R.D. Adams, F.A. Cotton (Eds.), Catalysis by Di- and Polynuclear Metal Cluster Complexes, Wiley–VCH, New York, 1998.
[16] P. Braunstein, L.A. Oro, P.R. Raithby (Eds.), Metal Clusters in Chemistry, Wiley–VCH, Weinheim, 1999.
[17] M.I. Bruce, in: D.F. Shriver, H.D. Kaesz, R.D. Adams (Eds.), The Chemistry of Metal Cluster Complexes, VCH, New York, 1990, p. 367.
[18] M.I. Bruce, in: P. Braunstein, L.A. Oro, P.R. Raithby (Eds.), Metal Clusters in Chemistry, vol. 3, Wiley–VCH, Weinheim, 1999, p. 1711.
[19] K. Wade, Adv. Inorg. Chem. Radiochem. 18 (1976) 1.
[20] D.M.P. Mingos, A.S. May, in: D.F. Shriver, H.D. Kaesz, R.D. Adams (Eds.), The Chemistry of Metal Cluster Complexes, VCH Publishers, New York, 1990, p. 11.
[21] G. Ciani, A. Sironi, J. Organomet. Chem. 241 (1983) 385.
[22] B.K. Teo, Inorg. Chem. 23 (1984) 1251.
[23] B.K. Teo, N.J.A. Sloane, Inorg. Chem. 24 (1985) 4545.
[24] R.J. Doedens, L.F. Dahl, J. Am. Chem. Soc. 88 (1966) 4847.
[25] P. Corradini, J. Chem. Phys. 31 (1959) 1676.
[26] M.R. Churchill, J.P. Hutchinson, Inorg. Chem. 17 (1978) 3528.
[27] G. Doyle, K.A. Eriksen, D. Van Engen, J. Am. Chem. Soc. 107 (1985) 7914.
[28] P.F. Jackson, B.F.G. Johnson, J. Lewis, W.J.H. Nelson, M. McPartlin, J. Chem. Soc. Dalton Trans. (1982) 2099.
[29] D. Collini, S. Fedi, C. Femoni, F. Kaswalder, M.C. Iapalucci, G. Longoni, P. Zanello, J. Cluster Sci. 16 (2005) 455.

[30] L.H. Gade, B.F.G. Johnson, J. Lewis, M. McPartlin, H.R. Powell, P.R. Raithby, W.T. Wong, J. Chem. Soc., Dalton Trans. 4 (1994) 521.

[31] M. Kawano, J.W. Bacon, C.F. Campana, B.E. Winger, J.D. Dudek, S.A. Sirchio, S.L. Scruggs, U. Geiser, L.F. Dahl, Inorg. Chem. 40 (2001) 2554.

[32] P. Zanello, Coord. Chem. Rev. 83 (1988) 199.

[33] P. Zanello, Coord. Chem. Rev. 87 (1988) 1.

[34] P. Lemoine, Coord. Chem. Rev. 47 (1982) 56.

[35] P. Lemoine, Coord. Chem. Rev. 83 (1988) 169.

[36] W.B. Geiger, Prog. Inorg. Chem. 33 (1985) 275.

[37] S.R. Drake, Polyhedron 9 (1990) 455.

[38] P. Zanello, in: P. Zanello (Ed.), Stereochemistry of Organometallic and Inorganic Compounds, vol. 5, Elsevier, Amsterdam, 1994, p. 163.

[39] P. Zanello, Structure and Bonding, vol. 79, Springer, Berlin, 1992, p. 101.

[40] P. Zanello, F. Fabrizi De Biani, in: P. Braunstein, L.A. Oro, P.R. Raithby (Eds.), Metal Clusters in Chemistry, vol. 2, Wiley–VCH, Weinheim, 1999, p. 1104.

[41] P. Zanello, in: P.I. Bernal (Ed.), Stereochemistry of Organometallic and Inorganic Compounds, vol. 4, Elsevier, Amsterdam, 1990, p. 181.

[42] G. Longoni, C. Femoni, M.C. Iapalucci, P. Zanello, in: P. Braunstein, L.A. Oro, P.R. Raithby (Eds.), Metal Clusters in Chemistry, vol. 2, Wiley–VCH, Weinheim, 1999, p. 1137.

[43] F. Calderoni, F. Demartin, M.C. Iapalucci, G. Longoni, P. Zanello, Inorg. Chem. 35 (1996) 898.

[44] V.G. Albano, R. Aureli, M.C. Iapalucci, F. Laschi, G. Longoni, M. Monari, P. Zanello, J. Chem. Soc. Chem. Commun. (1993) 1501.

[45] G. Longoni, M. Manassero, M. Sansoni, J. Am. Chem. Soc. 102 (1980) 7974.

[46] R.C. Adams, et al., Polyhedron 8 (1989) 2521.

[47] R. Della Pergola, L. Garlaschelli, C. Mealli, D.M. Proserpio, P. Zanello, J. Cluster Sci. 1 (1990) 93.

[48] R.D. Adams, M.S. Alexander, J. Arafa, W. Wu, Inorg. Chem. 30 (1991) 4717.

[49] A. Cinquantini, P. Zanello, R. Della Pergola, L. Garlaschelli, S. Martinengo, J. Organomet. Chem. 412 (1991) 215.

[50] S.R. Drake, B.F.G. Johnson, J. Lewis, R.C.S. McQueen, J. Chem. Soc. Dalton Trans. (1987) 1051.

[51] S.R. Drake, M.H. Barley, B.F.G. Johnson, J. Lewis, J. Chem. Soc. Chem. Commun. (1987) 1657.

[52] S.R. Drake, M.H. Barley, B.F.G. Johnson, J. Lewis, Organometallics 7 (1988) 806.

[53] G. Longoni, M. Manassero, M. Sansoni, J. Am. Chem. Soc. 102 (1980) 7973.

[54] E. Brivio, A. Ceriotti, R. Della Pergola, L. Garlaschelli, F. Demartin, M. Manassero, M. Sansoni, P. Zanello, F. Laschi, B.T. Heaton, J. Chem. Soc. Dalton Trans. (1994) 3237.

[55] V.G. Albano, D. Braga, A. Fumagalli, S. Martinengo, J. Chem. Soc. Dalton Trans. (1985) 1137.

[56] V.G. Albano, D. Braga, P. Chini, G. Ciani, S. Martinengo, J. Chem. Soc. Dalton Trans. (1982) 645.

[57] A. Fumagalli, M. Costa, R. Della Pergola, P. Zanello, F. Fabrizi de Biani, P. Macchi, A. Sironi, Inorg. Chim. Acta 350 (2003) 187.

[58] R. Della Pergola, L. Garlaschelli, M. Manassero, N. Masciocchi, P. Zanello, Angew. Chem. Int. Ed. 32 (1993) 1347.

[59] A. Ceriotti, F. Demartin, B.T. Heaton, P. Ingallina, G. Longoni, M. Manassero, M. Marchionna, N. Masciocchi, J. Chem. Soc. Chem. Commun. (1989) 786.

[60] D.F. Rieck, R.A. Montag, T.S. McKechnie, L.F. Dahl, J. Am. Chem. Soc. 108 (1986) 1330.

[61] R.E. Des Enfants, J.A. Gavney, R.K. Hayashi, A.D. Rae, L.F. Dahl, J. Organomet. Chem. 383 (1990) 543.

[62] D.F. Rieck, J.A. Gavney, R.L. Norman, R.K. Hayashi, L.F. Dahl, J. Am. Chem. Soc. 114 (1992) 10369.

[63] P.D. Mlynek, L.F. Dahl, Organometallics 16 (1997) 1641.

[64] P.D. Mlynek, L.F. Dahl, Organometallics 16 (1997) 1655.

[65] L.D. Lower, L.F. Dahl, J. Am. Chem. Soc. 98 (1976) 5046.

[66] D.F. Rieck, A.D. Rae, L.F. Dahl, J. Chem. Soc. Chem. Commun. (1993) 585.

[67] V.G. Albano, F. Demartin, M.C. Iapalucci, G. Longoni, A. Sironi, V. Zanotti, J. Chem. Soc. Chem. Commun. (1990) 547.

[68] V.G. Albano, F. Demartin, M.C. Iapalucci, F. Laschi, G. Longoni, A. Sironi, P. Zanello, J. Chem. Soc. Dalton Trans. (1991) 739.

[69] V.G. Albano, F. Demartin, C. Femoni, M.C. Iapalucci, G. Longoni, M. Monari, P. Zanello, J. Organomet. Chem. 325 (2000) 593.

[70] V.G. Albano, F. Demartin, M.C. Iapalucci, G. Longoni, M. Monari, P. Zanello, J. Chem. Soc. Dalton Trans. (1992) 497.

[71] A.J. Kahaian, J.B. Thoden, L.F. Dahl, J. Chem. Soc. Chem. Commun. (1992) 353.

[72] J.P. Zebrowski, R.K. Hayashi, L.F. Dahl, J. Am. Chem. Soc. 115 (1993) 1142.

[73] D.M.P. Mingos, Z. Lin, J. Chem. Soc. Dalton Trans. (1988) 1657.

[74] R. Gautier, J.-F. Halet, J.-Y. Saillard, in: P. Braunstein, L.A. Oro, P.R. Raithby (Eds.), Metal Clusters in Chemistry, vol. 3, Wiley–VCH, Weinheim, 1999, p. 1643.

[75] G. Ciani, A. Sironi, S. Martinengo, J. Chem. Soc. Dalton Trans. (1982) 1099.

[76] D. Collini, C. Femoni, M.C. Iapalucci, G. Longoni, P.H. Svensson, P. Zanello, Angew. Chem. Int. Ed. 41 (2002) 3685.

[77] D. Collini, C. Femoni, M.C. Iapalucci, G. Longoni, P.H. Svensson, Inorg. Chim. Acta 350 (2003) 321.

[78] J.L. Vidal, L.A. Kapicak, J.M. Troup, J. Organomet. Chem. 215 (1981) C11.

[79] D. Collini, PhD Thesis, Bologna, 2004.

[80] S. Martinengo, G. Ciani, A. Sironi, P. Chini, J. Am. Chem. Soc. 100 (1978) 7096.

[81] H. Brunner, H. Cattey, W. Meier, Y. Mugnier, A.C. Stuckl, J. Wachter, R. Wanninger, M. Zabel, Chem. Eur. J. 9 (2003) 3796.

[82] V.G. Albano, A. Ceriotti, P. Chini, G. Ciani, S. Martinengo, W.M. Anker, J. Chem. Soc. Chem. Commun. (1975) 859.

[83] G. Ciani, A. Sironi, S. Martinengo, J. Chem. Soc. Dalton Trans. (1981) 519.

[84] G. Ciani, M. Moret, A. Sironi, S. Martinengo, J. Organomet. Chem. 363 (1989) 181.

[85] S. Martinengo, G. Ciani, A. Sironi, J. Chem. Soc. Chem. Commun. (1991) 26.

[86] S. Martinengo, G. Ciani, A. Sironi, J.C.S. Chem. Commun. (1980) 1140.

[87] V.G. Albano, M. Sansoni, P. Chini, S. Martinengo, D. Strumolo, J. Chem. Soc. Dalton Trans. (1976) 970.

[88] A. Fumagalli, S. Martinengo, G. Bernasconi, L. Noziglia, V.G. Albano, M. Monari, C. Castellari, Organometallics 19 (2000) 5149.

[89] G. Ciani, A. Magni, A. Sironi, S. Martinengo, J. Chem. Soc. Chem. Commun. (1981) 1280.

[90] J.L. Vidal, R.A. Fiato, L.A. Cosby, R.L. Pruett, Inorg. Chem. 17 (1978) 2574.

[91] S. Martinengo, G. Ciani, A. Sironi, J. Am. Chem. Soc. 102 (1980) 7564.

[92] J.L. Vidal, R.C. Schoening, J.M. Troup, Inorg. Chem. 20 (1981) 227.

[93] S. Martinengo, G. Ciani, A. Sironi, J. Chem. Soc. Chem. Commun. (1992) 1405.

[94] A. Fumagalli, S. Martinengo, G. Bernasconi, G. Ciani, D.M. Proserpio, A. Sironi, J. Am. Chem. Soc. 119 (1997) 1450.

[95] J.P. Zebrowski, R.K. Hayashi, A. Bjarnason, L.F. Dahl, J. Am. Chem. Soc. 114 (1992) 3121.

[96] C. Femoni, M.C. Iapalucci, G. Longoni, P.H. Svensson, J. Chem. Soc. Chem. Commun. (2000) 655.

[97] N.T. Tran, M. Kawano, L.F. Dahl, J. Chem. Soc. Dalton Trans. (2001) 2731.

[98] E.G. Mednikov, Yu.L. Slovokhotov, Yu.T. Struchkov, Metalloorg. Khim. 4 (1991) 123.

[99] E.G. Mednikov, N.K. Eremenko, Yu.L. Slovokhotov, Yu.T. Struchkov, J. Organomet. Chem. 301 (1986) C35.

[100] J.T. Whittayakun, N.T. Tran, D.R. Powell, L.F. Dahl, cited in ref. [102].

[101] E.G. Mednikov, Organomet. Chem. USSR 4 (1991) 433.

[102] E.G. Mednikov, Russ. Chem. Bull. 42 (1993) 1242.
[103] E.G. Mednikov, N.I. Kanteeva, Russ. Chem. Bull. 44 (1995) 163.
[104] E.G. Mednikov, N.K. Eremenko, Yu.L. Slovokhotov, Yu.T. Struchkov, J. Chem. Soc. Chem. Commun. (1987) 218.
[105] E.G. Mednikov, S.A. Ivanov, L.F. Dahl, Angew. Chem. Int. Ed. 42 (2003) 323.
[106] N.T. Tran, M. Kawano, D.R. Powell, L.F. Dahl, J. Am. Chem. Soc. 120 (1998) 10986.
[107] N.T. Tran, L.F. Dahl, Angew. Chem. Int. Ed. 42 (2003) 3533.
[108] N.T. Tran, D.R. Powell, L.F. Dahl, Angew. Chem. Int. Ed. 39 (2000) 4121.
[109] C. Femoni, M.C. Iapalucci, G. Longoni, P.H. Svensson, P. Zanello, F. Fabrizi De Biani, Chem. Eur. J. 10 (2004) 2318.
[110] N.T. Tran, M. Kawano, D.R. Powell, L.F. Dahl, J. Chem. Soc. Dalton Trans. (2000) 4138.
[111] R.C.B. Copley, C.M. Hill, D.M.P. Mingos, J. Cluster Sci. 6 (1995) 71.
[112] C. Femoni, M.C. Iapalucci, G. Longoni, P.H. Svensson, J. Wolowska, Angew. Chem. Int. Ed. Engl. 39 (2000) 1635.
[113] C. Femoni, M.C. Iapalucci, G. Longoni, P.H. Svensson, Unpublished.
[114] M. Kawano, J.W. Bacon, C.F. Campana, L.F. Dahl, J. Am. Chem. Soc. 118 (1996) 7869.
[115] J.M. Bemis, L.F. Dahl, J. Am. Chem. Soc. 119 (1997) 4545.
[116] J.A.K. Howard, J.L. Spencer, D.G. Turner, J. Chem. Soc. Dalton Trans. (1987) 259.
[117] S.S. Kurasov, N.K. Eremenko, Yu.L. Slovokhotov, Yu.T. Struchkov, J. Organomet. Chem. 361 (1989) 405.
[118] D.M. Washecheck, E.J. Wucherer, L.F. Dahl, A. Ceriotti, G. Longoni, M. Manassero, M. Sansoni, P. Chini, J. Am. Chem. Soc. 101 (1979) 6110.
[119] A. Ceriotti, N. Masciocchi, P. Macchi, G. Longoni, Angew. Chem. Int. Ed. 38 (1999) 3724.
[120] A. Ceriotti, P. Chini, G. Longoni, M. Marchionna, L.F. Dahl, R. Montag, D.M. Washecheck, XV Cong. Naz. Chim. Inorg., Bari (1982) A26.
[121] J.D. Roth, G.J. Lewis, X. Jiang, L.F. Dahl, M.J. Weaver, J. Phys. Chem. 96 (1992) 7219.
[122] A. Fumagalli, S. Martinengo, G. Ciani, J. Chem. Soc. Chem. Commun. (1983) 1381.
[123] A. Fumagalli, S. Martinengo, G. Ciani, N. Masciocchi, A. Sironi, J. Am. Chem. Soc. 31 (1992) 336.
[124] F. Demartin, C. Femoni, M.C. Iapalucci, G. Longoni, P. Macchi, Angew. Chem. Int. Ed. 38 (1999) 531.
[125] F. Demartin, C. Femoni, M.C. Iapalucci, G. Longoni, P. Zanello, J. Cluster Sci. 12 (2001) 61.
[126] A. Ceriotti, F. Demartin, G. Longoni, M. Manassero, M. Marchionna, G. Piva, M. Sansoni, Angew. Chem. Int. Ed. 24 (1985) 696.
[127] C. Femoni, M.C. Iapalucci, G. Longoni, P.H. Svensson, J. Chem. Soc. Chem. Commun. (2001) 1776.
[128] C. Femoni, M.C. Iapalucci, G. Longoni, P.H. Svensson, Chem. Commun. (2004) 2274.
[129] P.D. Mlynek, M. Kawano, M. Kozee, L.F. Dahl, J. Cluster Sci. 12 (2001) 313.
[130] V.G. Albano, L. Grossi, G. Longoni, M. Monari, S. Mulley, A. Sironi, J. Am. Chem. Soc. 114 (1992) 5708.
[131] V.G. Albano, F. Calderoni, M.C. Iapalucci, G. Longoni, M. Monari, P. Zanello, J. Cluster Sci. 6 (1995) 107.
[132] D. Collini, C. Femoni, M.C. Iapalucci, G. Longoni, Compt. Rend. Chim. 8 (2005) 1645.
[133] J. Zhang, L.F. Dahl, J. Chem. Soc. Dalton Trans. (2002) 1269.
[134] N.T. Tran, D.R. Powell, L.F. Dahl, J. Chem. Soc. Dalton Trans. (2004) 209.
[135] N.T. Tran, D.R. Powell, L.F. Dahl, J. Chem. Soc. Dalton Trans. (2004) 217.
[136] N.T. Tran, M. Kawano, R.K. Hayashi, R.D. Powell, C.F. Campana, L.F. Dahl, J. Am. Chem. Soc. 121 (1999) 5945.
[137] J.C. Calabrese, L.F. Dahl, P. Chini, G. Longoni, S. Martinengo, J. Am. Chem. Soc. 96 (1974) 2614.
[138] F. Calderoni, F. Demartin, F. Fabrizi de Biani, C. Femoni, M.C. Iapalucci, G. Longoni, P. Zanello, Eur. J. Inorg. Chem. (1999) 663.
[139] G.J. Lewis, J.D. Roth, R.A. Montag, L.K. Safford, X. Gao, S.-C. Chang, L.F. Dahl, M.J. Weaver, J. Am. Chem. Soc. 112 (1990) 2831.
[140] C. Femoni, M.C. Iapalucci, G. Longoni, P.H. Svensson, J. Chem. Soc. Chem. Commun. 18 (2001) 1776.
[141] F. Fabrizi de Biani, C. Femoni, M.C. Iapalucci, G. Longoni, P. Zanello, A. Cerotti, Inorg. Chem. 38 (1999) 3721.
[142] A. Ceriotti, A. Fait, G. Longoni, G. Piro, F. Demartin, M. Manassero, M. Sansoni, J. Am. Chem. Soc. 108 (1986) 8091.
[143] F. Calderoni, F. Demartin, M.C. Iapalucci, G. Longoni, Angew. Chem. Int. Ed. Engl. 35 (1996) 2225.
[144] C. Mealli, D.M. Proserpio, J. Chem. Educ. 66 (1990) 399.
[145] V.A. Spasov, K.M. Ervin, J. Chem. Phys. 109 (1998) 5344.
[146] A. Grushov, K.M. Ervin, J. Chem. Phys. 106 (1997) 9580.
[147] Y.Y. Yeo, L. Vattuone, D.A. King, J. Chem. Phys. 106 (1997) 1990.
[148] Y.Y. Yeo, L. Vattuone, D.A. King, J. Chem. Phys. 104 (1996) 3810.
[149] S.-C. Chung, S. Kruger, G. Pacchioni, N. Rösch, J. Chem. Phys. 102 (1994) 3695.
[150] M.R.A. Blomberg, C.B. Lebrilla, P.E.M. Siegbahn, Chem. Phys. Lett. 150 (1988) 522.
[151] J.D. Roth, G.J. Lewis, L.K. Safford, X. Jiang, L.F. Dahl, M.J. Weaver, J. Am. Chem. Soc. 114 (1992) 6159.
[152] A. Ceriotti, Personal communication.
[153] R.L. De Kock, Inorg. Chim. Acta 19 (1976) L27.
[154] Q. Xu, Coord. Chem. Rev. 231 (2002) 83.
[155] Q. Xie, E. Perez-Cordero, L. Echegoyen, J. Am. Chem. Soc. 114 (1992) 3977.
[156] R.S. Ingram, M.J. Hostetler, R.W. Murray, T.G. Schaaff, J.T. Khoury, R.L. Whetten, T.P. Bigioni, D.K. Guthrie, P.N. First, J. Am. Chem. Soc. 119 (1997) 9279.
[157] J.F. Hicks, A.C. Templeton, S. Chen, K.M. Sheran, R. Jasti, R.W. Murray, J. Debord, T.G. Schaaff, R.L. Whetten, Anal. Chem. 71 (1999) 3703.
[158] D.T. Miles, R.W. Murray, Anal. Chem. 75 (2003) 1251.
[159] B.M. Quinn, P. Liljeroth, V. Ruiz, T. Laaksonen, K. Kontturi, J. Am. Chem. Soc. 125 (2003) 6644.
[160] T.F. Fässler, in: P. Braunstein, L.A. Oro, P.R. Raithby (Eds.), Metal Clusters in Chemistry, vol. 3, Wiley–VCH, Weinheim, 1999, p. 1612.
[161] S. Ulvenlund, L. Bengtsson-Kloo, in: P. Braunstein, L.A. Oro, P.R. Raithby (Eds.), Metal Clusters in Chemistry, vol. 1, Wiley–VCH, Weinheim, 1999, p. 561.
[162] C.A. Reed, R.D. Bolskar, Chem. Rev. 100 (2000) 1075.
[163] E.N. Esenturk, J. Fettinger, B. Eichhorn, J. Chem. Soc. Chem. Commun. (2005) 247, and references therein.
[164] G. Downie, Z. Tang, A.M. Guloy, Angew. Chem. Int. Ed. 39 (2000) 338.
[165] G. Longoni, F. Morazzoni, J. Chem. Soc. Dalton Trans. (1981) 1735.
[166] J. Sinzig, L.J. de Jongh, A. Ceriotti, R. Della Pergola, G. Longoni, M. Stener, K. Albert, N. Rösch, Phys. Rev. Lett. 81 (1998) 3211.
[167] S.F.A. Kettle, E. Diana, R. Rossetti, P.L. Stanghellini, J. Am. Chem. Soc. 119 (1997) 8228.
[168] A. Sandell, J. Libuda, P.A. Brühwiler, S. Andersson, M. Bäumer, A.J. Maxwell, N. Mårtensson, H.-J. Freund, J. Phys. Rev. B 55 (1997) 7233.
[169] P.P. Edwards, in: J.A. Charles, G.C. Smith (Eds.), Advances in Physical Metallurgy, Institute of Metals, London, 1990, p. 93.
[170] K.J. Taylor, C.L. Pettiette-Hall, O. Cheshnovsky, R.E. Smalley, J. Chem. Phys. 96 (1992) 3319.
[171] H. Zhang, G. Schmid, U. Hartman, Nano Lett. 3 (2003) 305.
[172] L.H. Gade, B.F.G. Johnson, J. Lewis, M. McPartlin, H.R. Powell, J. Chem. Soc. Chem. Commun. (1990) 110.
[173] S. Zacchini, in preparation.
[174] M.A. Beswick, J. Lewis, P.R. Raithby, M.C. Ramirez de Arellano, Angew. Chem. Int. Ed. 36 (1997) 291.
[175] M.A. Beswick, J. Lewis, P.R. Raithby, M.C. Ramirez de Arellano, Angew. Chem. Int. Ed. 36 (1997) 2227.
[176] D.S. Shephard, T. Maschmeyer, B.F.G. Johnson, J.M. Thomas, G. Sankar, D. Ozkaya, W. Zhou, R.D. Oldroyd, R.G. Bell, Angew. Chem. Int. Ed. 36 (1997) 2242.

[177] B.T. Heaton, L. Strona, S. Martinengo, D. Strumolo, V.G. Albano, D. Braga, J. Chem. Soc. Dalton Trans. (1983) 2175.

[178] K.R. Nary, P.L. Kuhns, M.S. Conradi, Phys. Rev. B 26 (1982) 3370.

[179] M. Watanabe, P. Wissman, Surf. Sci. 138 (1984) 95.

[180] G. Schmid, Chem. Rev. 92 (1992) 1709.

[181] R.L. Whetten, J.T. Khoury, M.M. Alvarez, S. Murthy, I. Vezmar, Z.L. Wang, P.W. Stephens, C.L. Cleveland, W.D. Luedtke, U. Landman, Adv. Mater. 8 (1996) 428.

[182] J.D. Aiken III, R.G. Finke, J. Mol. Catal. A: Chem. 145 (1999) 1.

[183] H. Bönnemann, W. Brijoux, in: P. Braunstein, L.A. Oro, P.R. Raithby (Eds.), Metal Clusters in Chemistry, vol. 2, Wiley–VCH, Weinheim, 1999, p. 913.

[184] M.N. Vargaftik, N.Yu. Kozitsyna, N.V. Cherkashina, R.I. Rudy, D.I. Kochubey, I.I. Moiseev, in: P. Braunstein, L.A. Oro, P.R. Raithby (Eds.), Metal Clusters in Chemistry, vol. 3, Wiley–VCH, Weinheim, 1999, p. 1364.

[185] L.J. De Jongh, in: P. Braunstein, L.A. Oro, P.R. Raithby (Eds.), Metal Clusters in Chemistry, vol. 3, Wiley–VCH, Weinheim, 1999, p. 1434.

[186] P. Moriarty, Rep. Prog. Phys. 64 (2001) 297.

[187] M. Brust, C.J. Kiely, Colloids Surf. A: Physicochem. Eng. Asp. 202 (2002) 119.

[188] A. Roucoux, J. Schultz, H. Patin, Chem. Rev. 102 (2002) 3757.

[189] M.-C. Daniel, D. Astruc, Chem. Rev. 104 (2004) 293.

[190] G. Schmid, R. Pfeil, R. Boese, F. Brandermann, S. Meyer, G.H.M. Calis, J.W.A. Van der Velden, Chem. Ber. 114 (1981) 3634.

[191] M. Brust, M. Walker, D. Bethell, D.J. Schifrinn, R. Whyman, J. Chem. Soc. Chem. Commun. (1994) 801.

[192] G. Longoni, P. Chini, J. Am. Chem. Soc. 98 (1976) 7225.

[193] T. Nakajima, A. Ishiguro, Y. Wakatsuki, Angew. Chem. Int. Ed. 39 (2000) 1131.

[194] T. Nakajima, A. Ishiguro, Y. Wakatsuki, Angew. Chem. Int. Ed. 40 (2001) 1066.

[195] K.-F. Yung, W.-T. Wong, Angew. Chem. Int. Ed. 42 (2003) 553.

[196] F. Demartin, M.C. Iapalucci, G. Longoni, Inorg. Chem. 32 (1993) 5536.

[197] A. Fumagalli, M.C. Malatesta, A. Tentori, D. Monti, P. Macchi, A. Sironi, Inorg. Chem. 41 (2002) 76.

[198] I.O. Koshevoy, M. Haukka, T.A. Pakkanen, S.P. Tunik, P. Vainiotalo, Organometallics 24 (2005) 3516.

[199] K. Lee, H. Song, J.T. Park, Acc. Chem. Res. 36 (2003) 78.

[200] J.L. Segura, N. Martin, Chem. Soc. Rev. 29 (2000) 13.

[201] N. Dragoe, H. Shimotani, M. Hayashi, K. Saigo, A. de Bettencourt-Dias, A.L. Balch, Y. Miyake, Y. Achiba, K. Kitazawa, J. Organomet. Chem. 65 (2000) 3269.

[202] N. Dragoe, H. Shimotani, J. Wang, M. Iwaya, A. de Bettencourt-Dias, A.L. Balch, K. Kitazawa, J. Am. Chem. Soc. 123 (2001) 1294.

[203] L.V. Interrante, M.J. Hampden-Smith (Eds.), Chemistry of Advanced Materials: An Overview, Wiley–VCH, New York, 1998.

[204] D.W. Bruce, D. O'Hare (Eds.), Inorganic Materials, John Wiley and Sons, New York, 1999.

[205] J.M. Williams, Adv. Inorg. Chem. Radiochem. 26 (1983) 235.

[206] L. Brossard, M. Ribault, L. Valade, P. Cassoux, Physica B and C (Amsterdam) 143 (1986) 378.

[207] H. Tajima, M. Inokuchi, A. Cobayashi, T. Ohta, R. Kato, H. Cobayashi, H. Kuroda, Chem. Lett. (1993) 1235.

[208] L.B. Coleman, M.J. Cohen, D.J. Sandman, F.G. Yamagishi, A.F. Garito, A.J. Heeger, Solid State Commun. 12 (1973) 1125.

[209] K. Bechgaard, K. Carneiro, F.B. Rasmussen, H. Olsen, G. Rindorf, C.S. Jacobsen, H. Pedersen, J.E. Scott, J. Am. Chem. Soc. 103 (1981) 2440.

[210] A.F. Diaz, K.K. Kanazawa, G.P. Gardini, J. Chem. Soc. Chem. Commun. (1979) 635.

[211] J. Roncali, Chem. Rev. 92 (1992) 711.

[212] W.A. Little, Phys. Rev. A 134 (1964) 1416.

[213] D. Jerome, K. Bechgaard, Nature 410 (2001) 162.

[214] J.K. Bera, K.R. Dunbar, Angew. Chem. Int. Ed. 41 (2002) 4453.

[215] G.M. Finniss, E. Canadell, C. Campana, K.R. Dunbar, Angew. Chem. Int. Ed. Engl. 35 (1996) 2772.

[216] F. Huq, A.C. Skapski, J. Cryst. Mol. Struct. 4 (1974) 411.

[217] F. Bagnoli, D. Belli Dell'Amico, F. Calderazzo, U. Englert, F. Marchetti, G.E. Herberich, N. Pasqualetti, S. Ramello, J. Chem. Soc. Dalton Trans. (1996) 4317.

[218] F.A. Cotton, E.V. Dikarev, M.A. Petrukhina, J. Organomet. Chem. 596 (2000) 130.

[219] F.A. Cotton, E.V. Dikarev, M.A. Petrukhina, J. Chem. Soc. Dalton Trans. (2000) 4241.

[220] P. Klüfers, Angew. Chem. Int. Ed. 24 (1985) 70.

[221] N. Masciocchi, M. Moret, P. Cairati, F. Ragaini, A. Sironi, J. Chem. Soc. Dalton Trans. (1993) 471.

[222] W.R. Hastings, M.C. Baird, Inorg. Chem. 25 (1986) 2913.

[223] J.C. Calabrese, L.F. Dahl, A. Cavalieri, P. Chini, G. Longoni, S. Martinengo, J. Am. Chem. Soc. 96 (1974) 2616.

[224] D. Braga, F. Grepioni, P. Milne, E. Parisini, J. Am. Chem. Soc. 115 (1993) 5115.

[225] C.J. McNeal, J.M. Hughes, G.J. Lewis, L.F. Dahl, J. Am. Chem. Soc. 113 (1991) 372.

[226] P.M.S. Monk, The Viologens, John Wiley and Sons, Chichester, 1998, and references therein.

[227] D. Collini, C. Femoni, M.C. Iapalucci, G. Longoni, Proceedings of the II National Conference on Nanosciences and Nanotechnologies, Bologna, 2004, P1.12.

[228] D.J. Underwood, R. Hoffmann, K. Tatsumi, A. Nakamura, Y. Yamamoto, J. Am. Chem. Soc. 107 (1985) 5968.

[229] M.-H. Whangbo, Acc. Chem. Res. 16 (1983) 95.

[230] C. Femoni, F. Kaswalder, M.C. Iapalucci, G. Longoni, M. Mehlstaübl, S. Zacchini, in preparation.

[231] C.E. Plechnik, S. Liu, X. Chen, E.A. Meyers, S.G. Shore, J. Am. Chem. Soc. 126 (2004) 204.

[232] P. Feng, X. Bu, N. Zheng, Acc. Chem. Res. 38 (2005) 293.

[233] P. Cassoux, J.S. Miller, in: L.V. Interrante, M.J. Hampden-Smith (Eds.), Chemistry of Advanced Materials: An Overview, Wiley–VCH, New York, 1998, p. 19.

[234] V.G. Albano, C. Castellari, C. Femoni, M.C. Iapalucci, G. Longoni, M. Monari, S. Zacchini, J. Cluster Sci. 12 (2001) 75.

[235] V.G. Albano, L. Grossi, G. Longoni, M. Monari, S. Mulley, A. Sironi, J. Am. Chem. Soc. 114 (1992) 5708.

[236] T.M. Bockman, J.K. Kochi, J. Organomet. Chem. 55 (1990) 4127.

[237] T. Fujimoto, A. Fukuoka, J. Nakamura, M. Ichikawa, J. Chem. Soc. Chem. Commun. (1989) 845.

[238] T. Sawitowski, S. Franzka, N. Beyer, M. Levering, G. Schmid, Adv. Funct. Mater. 11 (2001) 169.

[239] G. Schmid, M. Baumle, N. Beyer, Angew. Chem., Int. Ed. 39 (2000) 181.

[240] S. Hoeppener, L. Chi, H. Fuchs, Nano Lett. 2 (2002) 459.

[241] G. Schmid, Y.-P. Liu, M. Schumann, T. Raschke, C. Radehaus, Nano Lett. 1 (2001) 405.

[242] G. Schmid, U. Simon, Chem. Commun. (2005) 697.

[243] V. Santhanam, J. Liu, R. Agarwal, R.P. Andres, Langmuir 19 (2003) 7881, and references therein.

[244] A.Y. Obydenov, S.P. Gubin, V.V. Khanin, S.N. Polyakov, A.N. Sergeyev-Cherenkov, E.S. Soldatov, A.S. Trifonov, G.B. Khomutov, Colloids and Surfaces: Phys, Eng. Asp. 198–200 (2002) 389.

[245] R.L. Carroll, C.D. Gorman, Angew. Chem. Int. Ed. 41 (2002) 4378.

[246] C. Li, W. Fan, B. Lei, D. Zhang, S. Han, T. Tang, X. Liu, Z. Liu, S. Asano, M. Meyyappan, J. Han, C. Zhou, Appl. Phys. Lett. 84 (2004) 1949.

[247] P. Vettiger, M. Despont, U. Drechsler, U. Dürig, W. Häberle, M.I. Lutwyche, H. Rothuizen, R. Stutz, R. Widmer, G.K. Binnig, IBM J. Res. Dev. 44 (2000) 323.

[248] D. Wouters, U.S. Schubert, Angew. Chem. Int. Ed. 43 (2004) 2480.

[249] M.H.V. Werts, M. Lambert, J.-P. Bourgoin, M. Brust, Nano Lett. 2 (2002) 43.

[250] B.T. Heaton, P. Ingallina, R. Devenish, C.J. Humphries, A. Ceriotti, G. Longoni, M. Marchionna, J. Chem. Soc. Chem. Commun. (1987) 765.

[251] R.W. Devenish, B.T. Heaton, G. Longoni, S. Mulley, Nanocrystalline Materials edited by Mater. Res. Soc. 237 (1990) 245.

[252] R. Devenish, B.T. Heaton, S. Mulley, G. Longoni, Mater.: Chem. Phys. 29 (1991) 467.

[253] M. Ichikawa, in: P. Braunstein, L.A. Oro, P.R. Raithby (Eds.), Metal Clusters in Chemistry, vol. 3, Wiley–VCH, Weinheim, 1999, p. 1273.

[254] B.F.G. Johnson, S.A. Reynor, D.B. Brown, D.S. Shephard, T. Mashmeyer, J.M. Thomas, S. Hermans, R. Raja, G. Sankar, J. Mol. Catal. A: Chem. 182–183 (2002) 89.

[255] J.M. Thomas, R. Raya, J. Organomet. Chem. 689 (2004) 4110.

[256] J.M. Thomas, B.F.G. Johnson, R. Raja, G. Sankar, P.A. Midgley, Acc. Chem. Res. 36 (2003) 20.

[257] P.J. Dyson, Coord. Chem. Rev. 248 (2004) 2443.